bioRxiv preprint doi: https://doi.org/10.1101/2020.05.04.075119; this version posted June 4, 2023. The copyright holder for this preprint (which was not certified by peer review) is the author/funder, who has granted bioRxiv a license to display the preprint in perpetuity. It is made available under aCC-BY-NC 4.0 International license.

Single-cell RNA sequencing reveals subset-specific functional reprogramming of CD4$^+$ T-cells from PLHIV upon *ex vivo* HDAC inhibition and biomarkers of cells harbouring non-silent proviruses

Julia Kazmierski[1,2,], Dylan Postmus[1,2], Emanuel Wyler[3], Jelizaveta Fadejeva[1,2], Thijs Steijaert[1,2], Cornelius Fischer[4], Jenny Jansen[1,2], Uwe Koppe[5], Barbara Gunsenheimer-Bartmeyer[5], Karolin Meixenberger[6], Sarah N. Vitcetz[4], Madlen Sohn[4], Lucie Loyal[7,8], Andreas Thiel[7,8], Sascha Sauer[4], Norbert Bannert[6], Markus Landthaler[3,9] and Christine Goffinet[1,2]

[1]Institute of Virology, Charité - Universitätsmedizin Berlin, Corporate Member of Freie Universität Berlin and Humboldt-Universität zu Berlin, Berlin, Germany

[2]Berlin Institute of Health (BIH), Berlin, Germany

[3]Berlin Institute for Medical Systems Biology, Max Delbrück Center for Molecular Medicine in the Helmholtz Association, Berlin, Germany.

[4]Scientific Genomics Platforms, Max Delbrück Center for Molecular Medicine in the Helmholtz Association, Berlin, Germany.

[5]Department of Infectious Disease Epidemiology, Robert Koch Institute, Berlin, Germany

[6]Sexually transmitted bacterial pathogens and HIV, Robert Koch Institute, Berlin, Germany.

[76]Si-M / “Der Simulierte Mensch” a science framework of Technische Universität Berlin and Charité - Universitätsmedizin Berlin, corporate member of Freie Universität Berlin, Humboldt-Universität zu Berlin, Berlin, Germany

[8]Regenerative Immunology and Aging, BIH Immunomics, Berlin Institute of Health, Berlin, Germany

[9]Institute for Biology, Humboldt-Universität zu Berlin, Berlin, Germany.

Christine Goffinet, Institute of Virology, Campus Charité Mitte, Charité - Universitätsmedizin Berlin, Charitéplatz 1, 10117 Berlin, Germany

bioRxiv preprint doi: https://doi.org/10.1101/2020.05.04.075119; this version posted June 4, 2023. The copyright holder for this preprint (which was not certified by peer review) is the author/funder, who has granted bioRxiv a license to display the preprint in perpetuity. It is made available under aCC-BY-NC 4.0 International license.

Phone: +0049 30 450 525 489

e-mail: christine.goffinet@charite.de

Keywords: HIV-1, single cell RNA-sequencing, latency, HDACi

ABSTRACT

Shock-and-kill is one of the most advanced, yet unrealized, concepts towards establishment of HIV-1 cure. Treatment with latency-reversing agents (LRAs), including histone deacetylase inhibitors (HDACis) exerting chromatin remodelling and gene expression reprogramming, combined with anti-retroviral therapy reactivates HIV-1 transcription *in vitro*, *ex vivo* and *in vivo*. However, LRA treatment so far failed to significantly reduce the size of the viral reservoir in people living with HIV-1 (PLHIV), indicating its insufficiency in terms of elimination of latently infected cells. Here, by combining single cell RNA-sequencing and functional approaches, we characterised HDACi treatment-induced alterations of $CD4^+$ T-cell subset composition, subpopulation-specific transcriptional profiles, and HIV-1 reactivation, using Vorinostat and Panobinostat as two prototypic HDACis. *Ex vivo* exposure of $CD4^+$ T-cells from three aviremic PLHIV with clinically applicable concentrations of Panobinostat, but not Vorinostat, markedly reduced the expression and functionality of genes mediating antiviral immunity and T-cell activation. These modulations occurred in a $CD4^+$ T-cell subset-specific manner, with an PLHIV-specific exhausted $CD4^+$ T-cell subset that was to a certain extent refractory to said gene modulations. Furthermore, specific cellular genes were differentially expressed in the small HIV-1 RNA-positive fraction of $CD4^+$ T-cells from PLHIV. In latently HIV-1-infected J1.1 T-cells, specific genes correlated positively and negatively with the abundance of HIV-1 transcripts at the single cell level. In sum, we present LRA treatment-imposed gene expression changes and their functional implications, and present a list of gene candidates that may serve as biomarkers of T-cells with active HIV-1 transcription.

bioRxiv preprint doi: https://doi.org/10.1101/2020.05.04.075119; this version posted June 4, 2023. The copyright holder for this preprint (which was not certified by peer review) is the author/funder, who has granted bioRxiv a license to display the preprint in perpetuity. It is made available under aCC-BY-NC 4.0 International license.

INTRODUCTION

Highly active antiretroviral therapy (HAART) effectively suppresses viremia and has improved the quality and duration of life of people living with HIV/AIDS (PLHIV). However, though viremia in optimally treated individuals is below detection limit, latently infected cells persist and expand[1]. Cessation of treatment ultimately results in a return to a viraemic state within weeks in the vast majority of PLHIV[2].

The HIV-1 reservoir is maintained by long-lived, latently infected $CD4^+$ T-cells and monocytic cells. A general consensus is that there is a higher frequency of latent HIV-1 proviruses in memory $CD4^+$ T-cells than in naïve $CD4^+$ T-cells *in vivo*[3,4], even though the initial establishment of latency may occur in both proliferating and resting $CD4^+$ T-cells[5] and in phenotypically distinct T-cell subsets [6]. Conclusions on the size of the viral reservoir and subset distribution must be differentiated depending on the specific method applied to quantify the presence of either total, intact and/or re-activatable HIV-1 genomes, and the nature and duration of the stimulus applied for *ex vivo* reactivation of latent HIV-1 proviruses, if any[7]. The viral reservoir displays a long half-life and slow decay rate, with estimated 73 years of optimal antiretroviral therapy theoretically required for eradication[8,9]. Mechanisms of persistence of the viral reservoir despite HAART include clonal expansion through antigen-driven and homeostatic proliferation involving cytokines, respectively, as evidenced by the majority of $CD4^+$ T-cells in treated PLHIV sharing identical HIV-1 genome sequences, integration sites[10–12], and TCR sequences[13].

The concept of the *shock-and-kill* cure approach is based on the administration of latency-reversing agents (LRAs), including histone deacetylase (HDAC) inhibitors, combined with antiretroviral treatment. The intention is to reverse proviral quiescence in cellular reservoirs, an event that should be followed by specific elimination of reactivating cells using

bioRxiv preprint doi: https://doi.org/10.1101/2020.05.04.075119; this version posted June 4, 2023. The copyright holder for this preprint (which was not certified by peer review) is the author/funder, who has granted bioRxiv a license to display the preprint in perpetuity. It is made available under aCC-BY-NC 4.0 International license.

immunological or exogenous pharmacological mechanisms[14,15]. Clinical trials addressing the ability of numerous individual LRAs to purge latent HIV-1 *in vivo* demonstrated increased levels of unspliced cell-associated HIV-1 RNA[16–18] and increased viremia[18,19] but no detectable reduction of the size of the viral reservoir in most study participants[16–19]. In most recent preclinical studies, neither use of AZD5582, an activator of the non-canonical NF-κB signaling pathway[20], nor antibody-mediated depletion of $CD8^+$ T-cells combined with administration of the drug N-803, an IL-15 activator[21], reduced the size of the pool of latently infected cells in animal models despite ample HIV-1 reactivation. Together, these findings illustrate an urgent need for conceptual improvement of the *shock-and-kill* approach.

It has been suggested that individual LRAs display distinct specificities and potencies with regard to different $CD4^+$ T-cell subpopulations[22], resulting in suboptimal responses in some, but not other subsets, depending on their respective basal gene expression program. Furthermore, we hypothesised that LRA treatment may, beyond the well-appreciated reactivation of HIV-1 transcription, be accompanied by insufficiently recognized pleiotropic effects with beneficial and/or disadvantageous consequences from the perspective of the *shock-and-kill* approach. Along this idea, PHA-mediated reactivation of latently infected $CD4^+$ T-cells from PLHIV were reported to result in differential expression of genes related to cellular antiviral immunity[13].

Here, we characterised the basal and HDACi-induced, cellular and viral, transcriptomic landscape of individual subsets in *ex vivo*-treated $CD4^+$ T-cells isolated from three aviremic PLHIV as compared to cells from an uninfected donor. Overall, HDACi treatment imposed a major subset-specific reduction of expression of type I interferon (IFN)-stimulated genes (ISG) and genes involved in T-cell receptor signalling and activation, each with functional implications during HIV-1 reactivation and immune recognition. Furthermore, scRNA-sequencing of CD4+ T-cell from PLHIV and of latently infected J1.1 T-cells revealed the prevalence, subset distribution, and differential gene expression profile of T-cells scoring positive for HIV-1 transcripts, suggesting that specific genes can potentially be exploited as biomarkers for cells supporting active transcription from the HIV-1 LTR.

bioRxiv preprint doi: https://doi.org/10.1101/2020.05.04.075119; this version posted June 4, 2023. The copyright holder for this preprint (which was not certified by peer review) is the author/funder, who has granted bioRxiv a license to display the preprint in perpetuity. It is made available under aCC-BY-NC 4.0 International license.

RESULTS

Panobinostat treatment modulates expression of CD4⁺ T-cell subset-specific markers

In order to characterise LRA-induced cellular responses and CD4⁺ T-cell subpopulation-specific susceptibilities to HDAC inhibition, we exposed purified CD4⁺ T-cells isolated from three aviremic PLHIV (**Supplementary Table 1**) to Vorinostat, Panobinostat, IL-2/PHA or left them mock-treated for 48 hours, followed by single cell RNA-sequencing. We selected Vorinostat and Panobinostat as prototypic HDACis due to their demonstrated ability to reactivate HIV-1 RNA expression *in vivo*[16,19]. The applied concentrations of Vorinostat (500 nM) and Panobinostat (50 nM) approached those detected in patients´ plasma after single oral administration[16,19,23,24]. We included IL-2/PHA treatment as a reference that we expected to result in maximal activation of T-cells.

In order to exclude the possibility of bias introduction during cell subtype identification based on cultivation, we first generated a dataset using freshly isolated CD4⁺ T-cells from an HIV-1-negative donor to identify the following T-cell subsets using previously defined marker genes[25–27]: Naïve (T_N), central memory (T_{CM}), transitory memory (T_{TM}), effector memory (T_{EM}), effector memory re-expressing CD45RA (T_{EMRA}) and regulatory (T_{REG}) T-cells (**Sup. Fig. 1A-B**). We next applied these markers to the mock-, HDACi- and IL-2/PHA-treated CD4⁺ T-cells of PLHIV (**Fig. 1A**). In line with previous studies[28], the T-cell subset distribution was not significantly altered in mock-treated samples from aviremic PLHIV undergoing HAART as compared to a culture from an HIV-1-negative donor (**Fig. 1B**). However, we confirmed the previously reported presence of a small subpopulation specifically identified in cells from PLHIV[28,29], characterised by a combined and significantly higher expression of the exhaustion markers *PDCD1*, *LAG3, HAVCR2, GZMB* that was clearly separated from the otherwise

bioRxiv preprint doi: https://doi.org/10.1101/2020.05.04.075119; this version posted June 4, 2023. The copyright holder for this preprint (which was not certified by peer review) is the author/funder, who has granted bioRxiv a license to display the preprint in perpetuity. It is made available under aCC-BY-NC 4.0 International license.

similar T_{EMRA} cells (**Sup. Fig. 2**). Accordingly, we referred to this subset as exhausted T-cells (T_{EX}).

Vorinostat-treated $CD4^+$ T-cell cultures displayed very mild changes in subset distribution. Specifically, Vorinostat treatment induced a moderate decrease (from 23.91% to 18.33%, p = 0.033) and increase (from 50.25% to 54.35%, p = 0.0088) in the proportion of cells positive for markers of T_{CM} and T_N cells, respectively, compared to mock-treated samples from the same donors, while other T-cell subsets were not affected (**Fig. 1B**). Panobinostat treatment induced a prominent shift in the apparent T-cell subset distribution, resulting in a complete loss of cells expressing markers of T_{TM} (9.34% to 0%, p = 0.0008), T_{EMRA} (5.03% to 0%, p = 0.0676) and T_{REG} (4.98% to 0%, p = 0.0161) subsets and a parallel increase in the proportion of T_{CM} (23.9% to 35.57%, p = 0.0155). Relative levels of T_N (50.25% to 54.34%, p = 0.0821), T_{EX} (0.43% to 1.11%, p = 0.778) and T_{EM} cells (6.06% to 5.18%, p = 0.2215) remained unchanged under these experimental conditions (**Fig. 1B**). Treatment with IL-2/PHA resulted, as expected, in a reduction of relative numbers of T_N cells (50.25% to 34.96%, p = 0.0249), and a complete loss of the T_{EX}-cell population (0.42% to 0%, p = 0.313). Relative numbers of T_{CM} (23.91% to 30.58%, p = 0.0305) and T_{EM} cells (6.05% to 16.2%, p = 0.0383) increased, in line with potent, nonspecific T-cell activation. The observed changes in the T-cell subset distribution induced by the individual treatments were detected in cell cultures from all three donors to a similar extent (**Sup. Fig. 3A**) and Principal Component Analysis (PCA) confirmed that the respective *ex vivo* treatment, rather than donor-specific properties, determined the global transcriptomic state of a sample (**Sup. Fig. 3B**).

To corroborate and further investigate the HDACi-induced changes in marker RNA expression, with a special emphasis on the loss of cells expressing marker RNAs of T_{TM}, T_{EMRA} and T_{REG}-cells upon Panobinostat treatment, we analysed cell viability and cell surface expression of selected T-cell protein markers on $CD4^+$ T-cells isolated from uninfected individuals by flow cytometry (**Sup. Fig. 4**). Treatment with Panobinostat resulted in an increased percentage of cells displaying signs of early and late apoptotic cell death, in comparison to mock treatment of cell cultures from the same donors. Vorinostat treatment

bioRxiv preprint doi: https://doi.org/10.1101/2020.05.04.075119; this version posted June 4, 2023. The copyright holder for this preprint (which was not certified by peer review) is the author/funder, who has granted bioRxiv a license to display the preprint in perpetuity. It is made available under aCC-BY-NC 4.0 International license.

induced a similar trend, however without reaching statistical significance regarding late apoptotic cells (**Sup. Fig. 4A-B**). Although changes detected were statistically significant in Panobinostat-treated samples, we consider them unlikely to explain the complete loss of T_{TM}, T_{EMRA} and T_{REG} RNA marker-expressing cells.

Next, we quantified the expression of selected T-cell subset and activation markers as well as cytokine receptors (**Sup. Fig. 4C**). In line with the transcriptomic data, no major changes in surface protein expression were detectable in Vorinostat-treated cells, as compared to mock-treated cells, with the notable exception of a slightly reduced expression of the resting T-cell marker CD62L[30] and mild upregulation of CD69. In stark contrast, cell surface expression of multiple T-cell markers was significantly reduced upon Panobinostat treatment, including CD3, CD4, CD45RA (marker for naïve T-cells), CD62L (SELL), CD45RO (marker for memory T-cells), HLA-DR (late marker for activated T-cells), CXCR4, and most pronounced, the cytokine receptor IL7R/CD127. CCR5 and CD69 cell surface expression, however, were mildly and statistically significantly increased in the context of Panobinostat treatment. In line with previous reports describing a transient induction of surface CD69 expression on peripheral $CD4^+$ and $CD8^+$ T-cells of patients treated with Panobinostat *in vivo*[31] and on *ex-vivo* Panobinostat-treated PBMCs from healthy donors[24], we confirmed strong, but transient increase of CD69 expression in $CD4^+$ T-cells when analysing its expression in a time-dependent manner (**Sup. Fig. 4D**).

Together, among the two HDACi treatments conducted under indicated experimental conditions, Panobinostat induced a massive rearrangement of $CD4^+$ T-cell subset marker expression.

Panobinostat treatment induces broad transcriptional down-modulation of genes involved in T-cell signalling and innate immunity

Analysis of differentially expressed genes (DEGs) revealed that Vorinostat treatment induced modest gene expression changes, with expression of 1.388 genes induced and 312 genes

bioRxiv preprint doi: https://doi.org/10.1101/2020.05.04.075119; this version posted June 4, 2023. The copyright holder for this preprint (which was not certified by peer review) is the author/funder, who has granted bioRxiv a license to display the preprint in perpetuity. It is made available under aCC-BY-NC 4.0 International license.

decreased (**Fig. 2A**). In contrast, Panobinostat treatment altered the expression of a total of 10.119 genes (5.327 up- and 4.872 down-regulated genes). Comparing the two HDACi treatments, 4.078 genes were up-regulated and 5.124 were down-regulated in Panobinostat-treated compared to Vorinostat-treated cells (**Fig. 2A**). Focussing on genes with >2-fold change in expression, cultures treated with individual HDACis displayed a substantial overlap of both up- and down-regulated genes, suggesting that transcriptomic alterations were partially similar (**Fig. 2B**). Gene set enrichment analysis revealed that gene sets previously associated to Notch signaling, synaptic vesicle trafficking and Alzheimer's disease-presenilin were enriched in Panobinostat-treated cell cultures (**Fig. 2C**), as a result of the high expression of ribosomal proteins (e.g. *RPS24*, *RPL23*, *RPL7*) specifically in T_N- and T_{CM}-cells, and histones (e.g. *HIST1H1D*, *H1F0*, *H1FX*), transcription factors (e.g. *JUN*, *KLF2*, *SOX4*), translation factors (e.g. *EIF3K, EEF2, ELOB*) and heat shock proteins (e.g. *HSPA2, HSPA1B*) specifically in T_{EM} and T_{EX}-cells (**Sup. Fig. 5**). Interestingly, the small subset of T_{EX}-cells exhibited the most prominent transcriptional remodulation upon Panobinostat treatment as judged by the induced expression fold changes. More specifically, we identified more than 190 genes to be highly expressed in the absence of treatment in T_{EX}-cells as compared to other T-cell subsets, such as *ZBED2*, *IL2RA*, *LTA* and *TNFRSF4,* whose expression was drastically decreased after Panobinostat treatment (**Sup. Fig. 5 middle box**). In contrast, a small number of genes was highly upregulated in Panobinostat-treated T_{EX}-cells, including genes encoding transcription factors, such as AP-1 (*JUN*, *JUNB*, *JUND*) or Immediate Early Response 2 (*IER2*) (**Sup. Fig. 5 bottom box**).

Pathways that were downregulated in the context of Panobinostat treatment were associated with T-cell activation, cytokine- and chemokine-mediated inflammation and JAK/STAT signalling (**Fig. 2C**), in line with reduced activity of multiple transcription factors essential for mediating innate and T-cell-specific immune responses, such as IRF9, STAT1, STAT2, NFKB1 and STAT5, GATA3, RELA, respectively (**Fig. 2D**). Interestingly, activity scores of IRF3 and STAT6 were increased in T_N and T_{CM} subsets (**Fig. 2D**), suggesting partial activation of innate signalling cascades upon Panobinostat treatment. Vorinostat, in contrast

bioRxiv preprint doi: https://doi.org/10.1101/2020.05.04.075119; this version posted June 4, 2023. The copyright holder for this preprint (which was not certified by peer review) is the author/funder, who has granted bioRxiv a license to display the preprint in perpetuity. It is made available under aCC-BY-NC 4.0 International license.

to Panobinostat treatment, failed to enrich or deplete specific gene sets, corroborating the minor impact of Vorinostat at the applied concentration on the overall T-cell transcriptomic profile.

Next, we analysed the expression profile of selected ISGs (**Fig. 2E-F**). In mock-treated samples, expression of individual ISGs was, to a certain extent, subset-specific (**Fig. 2E**). For example, *LGALS3BP* and *IFI44L* displayed the highest expression in resting T_N- and T_{CM}-cell subsets, respectively, while *OASL* and *APOBEC3G* expression was highest in T_{EM} and T_{EMRA} cells. T_{REG} cells expressed high levels of *GBP5* and moderate levels of other ISGs, while T_{EX} were characterised by high *IFNG* expression and low levels of several ISGs, among others *IFIT3* and *IFI6*. The observations on the individual ISG expression level were corroborated by the IFN Module Score that takes into account expression of multiple genes associated with IFN signalling. T_N-, T_{CM}- and T_{TM}-cells displayed an overall modest, T_{EM}-, T_{EMRA}- and T_{REG}-cells gradually increasing and T_{EX}-cells a relatively low IFN Module Score (**Fig. 2F**). Overall, Vorinostat treatment only mildly affected the ISG expression pattern and IFN Module Score (**Fig. 2E-F**), with most pronounced changes being enhanced expression of *IFI6* and *IFIT2* in T_{EMRA}-cells as well as of *IFI27*, *IFI44L*, *ISG15* and *IFITM1* in T_{EX}-cells. In contrast, Panobinostat-exposed $CD4^+$ T-cells displayed drastically decreased levels of the majority of ISGs, including *ISG20*, *MX1*, *IFI44L*, *IFITM1*, *XAF1*, *GBP2*, *IFI16* throughout all subsets and reduced expression of *IFI27*, *IFITM3*, *IFIT3*, *IFIT2* and *BST2* in T_N-, T_{CM}- and T_{EM}-cells, with an opposite trend in T_{EX}-cells (**Fig. 2E**). However, *IFIT1* and *STAT1* expression was increased after Panobinostat treatment in all subsets and was most pronounced in T_{EX}-cells. *IFI30* and *RASD2* expression was particularly induced in T_{EM}-cells (**Fig. 2E**). In conclusion, the IFN Module Score was decreased in Panobinostat-treated cells while it was largely maintained upon Vorinostat treatment (**Fig. 2F**).

As expected under mock treatment conditions, expression of genes whose products regulate and mediate T-cell signalling and activation was clearly T-cell subset-specific (**Fig. 2G-H**). Expression of *ZAP70*, *NFATC2* and *STAT4* was elevated in T_{EM}- and even more in T_{EMRA}-cells. T_{REG}-cells displayed specifically high expression of *MAP3K1*, *IL6R*, *SELL* and

bioRxiv preprint doi: https://doi.org/10.1101/2020.05.04.075119; this version posted June 4, 2023. The copyright holder for this preprint (which was not certified by peer review) is the author/funder, who has granted bioRxiv a license to display the preprint in perpetuity. It is made available under aCC-BY-NC 4.0 International license.

HLA-DRA, while exhausted T-cells expressed drastically increased levels of *IL2RA*, *NFKB1*, *STAT5A* and *CD28*. Vorinostat-treated CD4$^+$ T-cells harboured a largely conserved expression pattern of the selected genes, with exception of increased *CD69* expression throughout all T-cell subsets and reduced expression of *IL2RA*, *NFKB1*, *STAT5A* and *CD28* in T_{EX}-cells, while *ZAP70*, *AKT3*, *CCR2* and *CCR5* expression was upregulated in T_{EX}-cells.

In stark contrast, Panobinostat treatment induced downregulation of expression of multiple T-cell function-specific genes, including *IL4R*, *LAT*, *IL6R*, *ZAP70*, and those for which we had detected reduced protein expression on cell surface (CD62L (*SELL*), HLA-DRA, CD45RA/CD45RO (*PTPRC*), IL7R, CCR5 and CD3 (*CD3G*)). Some T-cell-specific genes were specifically upregulated in T_{EX}-cells, including *CD4*, *MAP3K1*, *CSK* and *AKT3*. In accordance with the transient nature of CD69 expression upon Panobinostat treatment (**Sup. Fig. 4D**), *CD69* mRNA expression at 48 hours equaled those of mock-treated cells. The overall trend of reduced T-cell activation-specific gene expression was reflected in a T-cell Activation Module Score of Panobinostat-treated cells that was reduced to below the average of mock- and Vorinostat-treated cells (**Fig. 2H**).

In order to test to which extent HDACi-imposed gene expression changes are preserved in a more amenable HIV-1 latency cell system, we treated J1.1 T-cells, an established immortalised cell model of HIV-1 latency, that harbour at least two replication-competent HIV-1 LAI proviruses per cell[32,33] with Vorinostat and Panobinostat (**Sup. Fig. 6**). Here, we applied concentrations of HDACis (16 µM Vorinostat and 200 nM Panobinostat) that induced a similar degree of HIV-1 reactivation as judged by intracellular HIV-1 p24 CA expression (**Sup. Fig. 6A**). Both treatments resulted in a similar number of down- and upregulated genes (**Sup. Fig. 6B**) with a substantial overlap of modulated genes (**Sup. Fig. 6C**). The different concentrations of applied Vorinostat (500 nM in the primary CD4$^+$ T-cells and 16 µM in J1.1 T-cells) precluded a fair comparison of Vorinostat-induced gene expression changes in these two cell systems. In contrast, the concentration of applied Panobinostat in J1.1 T-cells (200 nM) approached the one used in primary CD4$^+$ T-cells (50 nM) and induced partially similar gene expression changes. Specifically, upregulated and downregulated

bioRxiv preprint doi: https://doi.org/10.1101/2020.05.04.075119; this version posted June 4, 2023. The copyright holder for this preprint (which was not certified by peer review) is the author/funder, who has granted bioRxiv a license to display the preprint in perpetuity. It is made available under aCC-BY-NC 4.0 International license.

activity scores of transcription factors STAT6, FOXP1, IRF3, and STAT2, STAT4, IRF1, IRF4, GATA3, respectively, were conserved in both cell systems upon Panobinostat treatment, while Panobinostat-mediated suppression of gene expression via STAT1, STAT5A, STAT5B, IRF9, NF-κB and RELA was lost in J1.1 T-cells (**Sup. Fig. 6D**), potentially related to the documented defect of J1.1 T-cells in IL-2 production and Ca^{2+} mobilisation after CD3 stimulation[32]. Overall, this is in line with a highly pronounced, overall down-regulation of genes related to T-cell signalling and activation, such as *CD3G*, *SELL*, *LAT*, *STAT5A* or *ZAP70* and a significantly reduced T-cell Activation Module Score (**Sup. Fig. 6E**), comparable to the transcriptional modulations observed in the primary $CD4^+$ T-cell dataset (**Fig. 2**). In contrast, individual genes whose expression was negatively affected upon Panobinostat treatment in primary $CD4^+$ T-cells were found to be upregulated after Vorinostat or Panobinostat treatment of J1.1 T-cells, including *CCR7*, *IL2RA*, *AKT3* or *HLA-DRA* (**Sup. Fig. 6E**). While Panobinostat-treated primary $CD4^+$ and J1.1 T-cells shared expression profiles of some ISGs (downregulation of *MX1*, *MX2*, *OAS1*, *XAF1*, *BST2*; upregulation of *GBP5*, *STAT1*, *IFIT1*), they differed regarding expression of *LGALS3BP*, *GBP2*, *IFI44L*, *OASL* (**Sup. Fig. 6F**), resulting in an overall elevated IFN Module Score in J1.1 T-cells as opposed to primary $CD4^+$ T-cells.

Conclusively, under these experimental conditions, Panobinostat, and, if applied at higher concentration, also Vorinostat, significantly reduced expression of several genes that are essential for T-cell-specific immune responses. Interestingly, large-scale suppression of ISG expression by Panobinostat in primary $CD4^+$ T-cells was not entirely preserved in J1.1 T-cells, hinting towards important differences regarding susceptibility to and consequences of HDAC inhibition between the primary T-cell and the immortalised T-cell model.

HDAC inhibition imposes a block to $CD4^+$ T-cell activation and type I IFN signalling

We hypothesised that HDACi-induced modulation of gene expression, some with $CD4^+$ T-cell subset-specific patterns, is of functional relevance for HIV-1 reactivation and immune

bioRxiv preprint doi: https://doi.org/10.1101/2020.05.04.075119; this version posted June 4, 2023. The copyright holder for this preprint (which was not certified by peer review) is the author/funder, who has granted bioRxiv a license to display the preprint in perpetuity. It is made available under aCC-BY-NC 4.0 International license.

recognition of reactivating cells. To investigate the result of HDACi treatment on T-cell activation, we pre-incubated $CD4^+$ T-cells from HIV-1-negative donors with HDACis prior to adding IL-2/PHA as a strong, unspecific stimulus for T-cell activation (**Fig. 3A**). Pre-incubation with DMSO or Vorinostat resulted in marked IL-2/PHA-triggered enhancement of the percentage of cells expressing the activation markers CD69, CD25, HLA-DR and also the exhaustion markers TIM-3 and PD-1, indicating successful T-cell activation. Conversely, Panobinostat pretreatment resulted in impaired induction of CD69 expression (0.49-fold changed), and in a complete lack of IL-2/PHA-mediated induction of expression of CD25, HLA-DR, TIM-3 and PD-1 (**Fig. 3A**). To study TCR-induced T-cell activation, we preincubated $CD4^+$ T-cells with HDACi followed by treatment with a universal peptide pool in combination with an anti-CD28 antibody. Expression of the early activation marker CD69 after TCR stimulation was slightly, but statistically significantly induced in Vorinostat- (1.65-fold) and to a higher extent in Panobinostat-pretreated samples (5.5-fold), suggesting efficient initiation of T-cell activation in the presence of both HDACis (**Fig. 3B**). Expression of the middle activation marker CD25, the exhaustion marker PD-1 and the late activation marker HLA-DRA increased upon TCR stimulation in the context of Vorinostat pretreatment (2.07-, 2.07- and 1.39-fold change, respectively), suggesting that weak HDAC inhibition does not prevent TCR-specific T-cell activation. However, expression of CD25 and HLA-DRA was severely reduced in Panobinostat-pretreated cultures (0.05- and 0.47-fold change, respectively), suggestive of abortive peptide-induced T-cell activation.

We next examined the impact of HDAC inhibition on type I IFN signalling and ISG expression. Specifically, we treated $CD4^+$ T-cells isolated from HIV-1-negative donors with DMSO, Vorinostat (8 µM) or Panobinostat (50 nM) in combination with increasing concentrations of IFN-α2a and assessed cell surface expression changes of BST-2 and changes of *IFIT1* and *MX2* gene expression (**Fig. 3C-D**). We applied an increased concentration of Vorinostat in these experiments to adjust for the inferior potency of Vorinostat compared to Panobinostat that has been reported in previous studies[24,34] and as observed by us and others[34] in terms of HIV-1 reactivation (**Fig. 6A**). Both Vorinostat and Panobinostat

bioRxiv preprint doi: https://doi.org/10.1101/2020.05.04.075119; this version posted June 4, 2023. The copyright holder for this preprint (which was not certified by peer review) is the author/funder, who has granted bioRxiv a license to display the preprint in perpetuity. It is made available under aCC-BY-NC 4.0 International license.

significantly dampened base-line BST-2 cell surface expression levels, and both tested concentrations (100 and 1000 IU/ml) of IFN-α2a failed to rescue the HDACi-imposed block to BST2 surface expression (**Fig. 3C**). Interestingly, mRNA expression levels of the two ISGs *IFIT1* and *MX2* showed a divergent phenotype. Individual treatment with Vorinostat and Panobinostat, as well as addition of IFN-α2a, induced and further amplified *IFIT1* mRNA expression, respectively (**Fig. 3D**). In contrast, *MX2* mRNA expression decreased in the context of HDACi treatment, both in the absence and presence of 1000 IU/ml IFN-α2a (**Fig. 3E**), reminiscent of the profile observed for BST-2 expression (**Fig. 3C**). Of note, while type I IFN signalling is essential for induction of *MX2* expression, it is dispensable for induction of expression of *IFIT1* that is a direct target of IRF3-regulated transcription[35], a transcription factor that we found to display higher activity upon Panobinostat treatment. HDAC inhibition in the latently infected J1.1 T-cell line reverted prior IFN-α2a-induced expression of MX2 in a dose-dependent manner and abolished the negative impact of IFN on HIV-1 reactivation. In contrast, in cells treated with Bryostatin, a non-HDACi LRA that acts as a PKC agonist[36,37], IFN-induced MX2 expression was intact and accompanied by impaired HIV-1 reactivation (**Sup. Fig. 7A)**. Co-administration of increasing doses of IFN-α2a up to 10,000 IU/ml was insufficient to counteract the HDACi-suppressed MX2 expression and did not limit the efficiency of HIV-1 reactivation. In contrast, in the context of Bryostatin treatment, IFN treatment induced MX2 expression efficiently and inhibited HIV-1 reactivation in a dose-dependent fashion (**Sup. Fig. 7B**). In combination with the scRNA-seq datasets (**Fig. 2A-F**), these data suggest that, while IRF3-driven expression of a small subset of ISGs remains intact and is even exacerbated, HDAC inhibition is accompanied by dampened JAK/STAT-specific responses, resulting in downregulation of expression of IFN-regulated ISGs and facilitated HIV-1 reactivation.

Together, HDAC inhibition renders $CD4^+$ T-cells largely refractory, and/or less sensitive, to mitogen and TCR stimulation and dampens the base-line and IFN-induced expression of multiple ISGs, including the two prototypic ISGs *BST-2* and *MX2*. In conclusion,

bioRxiv preprint doi: https://doi.org/10.1101/2020.05.04.075119; this version posted June 4, 2023. The copyright holder for this preprint (which was not certified by peer review) is the author/funder, who has granted bioRxiv a license to display the preprint in perpetuity. It is made available under aCC-BY-NC 4.0 International license.

HDAC inhibition down-regulates distinct pathways essential for functional T-cell activation and innate immunity.

HIV-1 RNA abundance correlates with specific cellular gene expression in J1.1 T-cells

We next attempted to identify cellular genes whose expression correlates with HIV-1 mRNA abundance in a fashion that is independent of the mode of transcriptional reactivation. In the J1.1 T-cell line model, each individual cell harbours at least two integrated, reactivatable proviruses[32,33]. As expected due to HIV-1 p24 capsid protein positivity in 10-15% mock-treated J1.1 T-cells (**Suppl. Fig. 6A**), HIV-1 RNA was detected at base-line levels in most and at elevated levels in a minority of DMSO-treated cells. Vorinostat and Panobinostat treatment enhanced quantities of HIV-1 reads per cell, as expected (**Fig. 4A**). Due to fragmentation of nucleic acid molecules during library preparation, reads used for alignment to the viral RNA sequence of HIV-1 LAV-1[38] displayed a length of 91 bps. Our 3´-sequencing approach is largely restricted to the detection of polyadenylated viral mRNAs without allowing to differentiate whether transcripts originate from full-length, replication-competent or partially deleted, replication-competent proviral sequences. The majority of retrieved transcripts mapped to the HIV-1 5´- and 3´-LTR sequences (**Fig. 4B**), as expected given transcriptional initiation at the LTR regions. The two additional most prominent read accumulations at the 5' end of Pol and Tat probably reflect internal priming during polyA-based catching at A-rich sequences (Ann Emery and Ron Swanstrom, personal communication).

Using unsupervised clustering, 8 and 10 clusters were identified for Vorinostat/DMSO- and Panobinostat/DMSO-treated samples, respectively (**Fig. 4C**). Interestingly, we identified individual clusters of highly HIV-1 RNA-positive cells in the control conditions (cluster 4, DMSO I and cluster 5, DMSO II, (**Fig. 4C-D**)), in line with 10-15% of HIV-1 p24 capsid positivity observed in J1.1 T-cells at base-line conditions (**Suppl. Fig. 6A**). Upon HDAC inhibition, all cells displayed enhanced HIV-1 RNA expression, with highest levels in the clusters pre-

bioRxiv preprint doi: https://doi.org/10.1101/2020.05.04.075119; this version posted June 4, 2023. The copyright holder for this preprint (which was not certified by peer review) is the author/funder, who has granted bioRxiv a license to display the preprint in perpetuity. It is made available under aCC-BY-NC 4.0 International license.

expressing viral RNA at steady-state (**Fig. 4C-D**), indicating a virtual absence of cells being refractory to HDACi-mediated HIV-1 reactivation in the J1.1 T-cell culture.

We initially hypothesized that HIV-1 LTR transcription, followed by viral gene expression and synthesis of viral antigens stimulates expression of a multitude of cellular genes as a cellular response. Vice versa, it is possible that expression of specific, pre-expressed genes facilitated HIV-1 reactivation. Therefore, we aimed at identifying DEGs between cell populations displaying either high or low levels of HIV-1 RNA (HIV-1-high and HIV-1-low/negative). The thresholds of HIV-1-high and HIV-1-low were set for each treatment individually. The most pronounced change of gene expression between HIV-1 high and HIV-1-low groups was the over-representation of HIV-1 RNA by 12.96- and 15.6-fold in Vorinostat- and Panobinostat-treated cell cultures, respectively, and 4.35-4.57-fold in the two DMSO-treated cell cultures, validating our approach. The number of cellular, statistically significant DEGs between HIV-1-high and HIV-1-low cells within each treatment condition was limited to 3 (DMSO I), 83 (Vorinostat), 5 (DMSO II) and 278 genes (Panobinostat), each with only mild fold changes of expression (ranging from 0.73 to 2.0), but some displaying high statistical significance (**Supplementary Table 2, Fig. 4E**). These DEGs included *CBX5* and *DEAF1*, the two genes which serve as the two reported main integration sites in J1.1 T-cells[33,39]. We next analysed the top ten, most significant DEGs from all conditions to identify a potential negative or positive correlation with abundance of HIV-1 RNA, at single cell level, across all treatment conditions (**Fig. 4F-G**). Expression of these 34 genes displayed different degrees of correlation to HIV-1 RNA, some being treatment-specific. Expression of *CBX5*, *DEAF1*, *DHRS2* and three long non-coding RNAs, NEAT1, *MALAT1/NEAT2* and *LINC02158*, were found to strongly and statistically significantly correlate with HIV-1 RNA across all treatments (**Fig. 4G**), suggesting that their expression associates directly with HIV-1 RNA levels. Expression of *DHRS2* is induced upon acute HIV-1 infection of primary $CD4^+$ T-cells and controlled by a LTR12D endogenous retroviral element[40]. *MALAT1* was described as an enhancer of HIV-1 LTR-dependent transcription[41]. *NEAT1*, conversely, was suggested to be downregulated in the context of T-cell activation and to display antiviral functions[42].

bioRxiv preprint doi: https://doi.org/10.1101/2020.05.04.075119; this version posted June 4, 2023. The copyright holder for this preprint (which was not certified by peer review) is the author/funder, who has granted bioRxiv a license to display the preprint in perpetuity. It is made available under aCC-BY-NC 4.0 International license.

Expression of the histone-coding genes *HIST2H2AC*, *HIST1H1D*, *HIST1H1C* and *HNRNPU*, a gene encoding a nuclear phosphoprotein that potentially reduces the abundance of HIV-1 transcripts in the cytoplasm by targeting the 3´-LTR present on all viral RNA species[43], showed weak and absent correlation across all treatments, respectively (**Fig. 4G**).

Together, using an established cell line model of HIV-1 latency, our analysis uncovered a limited number of candidate genes whose expression tightly follows the HIV-1 transcriptional status.

Detection of HIV-1 RNA-positive CD4⁺ T-cells from PLHIV and their specific gene expression profile

To identify HIV-1-specific reads in CD4⁺ T-cells from PLHIV, we mapped all non-human reads to 14,609 complete HIV-1 genomes derived from the Los Alamos database (http://www.hiv.lanl.gov/). In the next step, all HIV-1 reference sequences that did not map CD4⁺ T-cell-derived sequences were removed and the remaining alignments, based on 52 reference HIV-1 genomes (**Supplementary Table 3**) were curated manually in order to exclude false-positive alignments that e.g. arose from degenerated sequence elements or multimappers. 156 reads in total from all samples were considered to correspond to HIV-1 sequences. CD4⁺ T-cells of PLHIV #2 displayed higher numbers of HIV-1-specific reads than donors 1 and 3 (**Fig. 5A**). The majority of HIV-1 reads from PLHIV #1 and #2 were detected in Panobinostat-treated cultures, while Vorinostat treatment resulted in highest HIV-1 read quantities in cells from PLHIV #3. Reminiscent of the coverage plot in J1.1 T-cells, and despite the more than 10.000-fold lower number of identified HIV-1 reads per cell in primary CD4⁺ T-cells as compared to J1.1 T-cells, a substantial fraction of the retrieved viral transcripts mapped to the 5'-LTR (**Fig. 5B**). In addition, we detected several internal peaks that we attribute to potential internal priming at A-rich sequences (Ann Emery and Ron Swanstrom, personal communication). HIV-1 RNA-positive T-cells spread throughout the UMAP projection (**Fig. 5C**). Importantly, absence of detectable HIV-1 reads in CD4⁺ T-cells obtained from an

bioRxiv preprint doi: https://doi.org/10.1101/2020.05.04.075119; this version posted June 4, 2023. The copyright holder for this preprint (which was not certified by peer review) is the author/funder, who has granted bioRxiv a license to display the preprint in perpetuity. It is made available under aCC-BY-NC 4.0 International license.

HIV-1-negative donor demonstrates the specificity and stringency of our approach. The proportion of HIV-1 RNA-positive T-cells was highest (7.5 cells per 10^4 $CD4^+$ T-cells) upon Panobinostat treatment, and lowest (2.2 cells per 10^4 $CD4^+$ T-cells) in the context of mock treatment (**Fig. 5D**), the latter suggesting incomplete silencing of the HIV-1 genome. The number of HIV-1-specific reads per cell varied between one and 14 (**Fig. 5E**). The T_{CM} (58.3%), followed by the T_N cell (30.6%) subset harbored the majority of HIV-1 RNA-positive cells (**Fig. 5F**). The only T_{EM}- and T_{EMRA}-cells that scored positive for HIV-1 RNA were identified in mock-treated cells. In order to identify cellular genes whose expression associates with HIV-1 RNA positivity, we compared the cellular transcriptional profile of all cells scoring HIV-1 RNA-positive with the one of all HIV-1 RNA-negative cells (**Fig. 5G**, upper panel, **Supplementary Table 4**). Applying an alternative strategy, we identified DEGs by iterative comparison of all HIV-1 RNA-positive cells with an equal number of randomly selected, treatment and cell type matched cells in 5.000 bootstrapped iterations (**Fig. 5G**, lower panel, **Supplementary Table 4**). In both analyses, *PSRC1*, *PLCD1* and *HES6* were identified as DEGs which were upregulated in HIV-1 RNA-positive cells. The matched analysis revealed several genes significantly downregulated in HIV-1 RNA-positive cells, including genes encoding the ESCRT component VPS4A involved in HIV-1 budding[44], the RNA-binding protein Staufen involved in HIV-1 RNA encapsidation[45,46] and the nuclear import cofactor Nup153[47]. In conclusion, by identifying individual HIV-1 RNA-positive $CD4^+$ T-cells, we provide their specific gene expression profile and identify a list of potential candidate genes which may either influence HIV-1 transcription and/or HIV-1 RNA stability or, vice versa, whose expression is modulated in the course of HIV-1 transcription.

DISCUSSION

The overarching aim of LRA treatment in the context of HIV-1 cure is reinitiation of HIV-1 mRNA and protein expression to a degree that is sufficient to render a maximum of reactivating cells immunologically visible, making them susceptible to elimination. The ability

bioRxiv preprint doi: https://doi.org/10.1101/2020.05.04.075119; this version posted June 4, 2023. The copyright holder for this preprint (which was not certified by peer review) is the author/funder, who has granted bioRxiv a license to display the preprint in perpetuity. It is made available under aCC-BY-NC 4.0 International license.

of HDACis to reverse HIV-1 latency *in vitro* and *in vivo*[16,18,19,24,48] involves hyperacetylation of histones, which leads to opening of cellular chromatin and subsequently modulation of gene expression, including transcriptional reactivation from dormant HIV-1 genomes and Tat-independent elongation of viral RNA[49,50]. LRA treatment *per se* influences the expression profile of a plethora of cellular genes, with to date poorly defined consequences on cellular processes affecting HIV-1 RNA stability, HIV-1 protein expression, trafficking and cell surface presentation, and finally susceptibility of reactivating cells to cytotoxicity. An optimal *shock-and-kill* regimen should, on the one hand, mount a proviral milieu that facilitates post-integration steps of the virus replication cycle. On the other hand, in a second step, an optimal *shock-and-kill* regimen must render reactivating cells susceptible to recognition and killing by $CD8^+$ T-cell and NK cell-mediated cytotoxicity, processes that are orchestrated in the target cell, among others, by functional type I IFN signalling [51,52].

Treatment of $CD4^+$ T-cells with Panobinostat resulted in the vanished expression of marker RNAs and cell surface markers of T_{TM}, T_{EMRA} and T_{REG} cells and a markedly impaired ability to respond to activation stimuli, including TCR/CD28 and IL-2/PHA, in line with reports of HDACi treatment-induced antigen-specific anergy of mouse lymphocytes[53]. As a notable exception, expression of the early activation marker CD69 was transiently induced upon *ex vivo* treatment of $CD4^+$ T-cells with Panobinostat, in line with other studies[24,31] and data obtained in T-cells derived from PLHIV following Panobinostat administration *in vivo*[24,31]. Given that Panobinostat treatment compromises functionality of NK cells[54] and $CD8^+$ T-cells[55,56], it is tempting to speculate that it also affects the efficiency of peptide processing and presentation in HIV-1-reactivating $CD4^+$ T-cells by MHC-I molecules. Along this line, HDACi treatment has been proposed to reduce cytosolic peptidase activities in *ex vivo*-HIV-1-infected $CD4^+$ T-cells, resulting in modulated antigen presentation to $CD8^+$ T-cells[57].

Of note, as opposed to treatment with 50 nM Panobinostat, 500 nM Vorinostat induced rather subtle, if any, changes in the $CD4^+$ T-cell subset composition and the cellular transcriptome of individual T-cell subpopulations. This lack of reprogramming is consistent with a study documenting absence of HIV-1 reactivation and immune activation in resting

bioRxiv preprint doi: https://doi.org/10.1101/2020.05.04.075119; this version posted June 4, 2023. The copyright holder for this preprint (which was not certified by peer review) is the author/funder, who has granted bioRxiv a license to display the preprint in perpetuity. It is made available under aCC-BY-NC 4.0 International license.

$CD4^+$ T-cells isolated from PLHIV treated with the identical concentration of Vorinostat [58]. Titration experiments in J1.1 T-cells showed that Vorinostat is roughly 10-fold less effective than Panobinostat in inducing HIV-1 reactivation, in line with previous studies[59,24]. However, clinically applicable regimen of Vorinostat are limited to nanomolar concentrations. A conservative calculation of Vorinostat concentrations in patients´ serum following a 400 mg drug administration estimated to be 340 nM[23]. Conclusively, our study, as well as other reports, used HDACi concentrations adapted from this calculation[58,60]. When using increasing concentrations of Vorinostat in the J1.1 T-cell line model, results approached those obtained with Panobinostat, suggesting that both HDACi share the qualitative ability to remodulate cellular transcription and gene expression programs when present at similar effective concentrations.

Our finding of reduced base-line expression of specific ISGs, and prevention of their induction by IFN, upon treatment with effective concentrations of HDACis, is in line with reports demonstrating facilitated HIV-1 infection of *ex vivo*-HDACi-treated $CD4^+$ T-cells[61,62]. HDACs, including HDAC4[63], HDAC6[62] and HDAC10[64], interfere with several steps of the HIV-1 replication cycle, and as a consequence, may be evaded by HIV-1 accessory gene products[65]. HDAC inhibition was demonstrated to block innate and inflammatory immune responses in multiple cell types[66,67], though to our best knowledge not yet in *ex vivo*-treated primary $CD4^+$ T-cells of PLHIV. Our data suggest that HDACi-induced establishment of a proviral intracellular milieu underlies the reported enhanced efficiency of HIV-1 *de novo* infection and, in latently infected cells, facilitates post-integration steps of the HIV-1 replication cycle beyond directly boosting HIV-1 transcriptional activity through remodulation of the HIV-1 LTR-containing chromatin region.

While Panobinostat treatment was followed by downregulation of the regulon activity of most studied transcription factors and an overall reduced IFN module score, expression of FOXP1-, IRF3- and STAT6-regulated genes was elevated in almost all $CD4^+$ T-cell subsets. The selective activation of these transcription factors potentially underlies the detected upregulation of *IFIT1*, *STAT1* and *GBP5* expression in several $CD4^+$ T-cell subsets. Beyond

bioRxiv preprint doi: https://doi.org/10.1101/2020.05.04.075119; this version posted June 4, 2023. The copyright holder for this preprint (which was not certified by peer review) is the author/funder, who has granted bioRxiv a license to display the preprint in perpetuity. It is made available under aCC-BY-NC 4.0 International license.

$CD4^+$ T-cell subset-specific expression of individual genes, the most striking observation was an overall refractoriness of the T_{EX} $CD4^+$ T-cells to Panobinostat-induced changes, illustrated by unchanged IFN signalling and T-cell activation module scores, probably due their already low level of expression of corresponding genes.

Vorinostat has been reported to specifically reactivate endogenous retroviruses of the LTR12 family[68,69]. In our own data, expression of *DHRS2*, a gene that was recently described to be fused upstream of the LTR12D gene locus and to be induced upon acute HIV-1 infection[40], displayed a strong correlation with HIV-1 mRNA expression across all treatment conditions in J1.1 T-cells, suggesting that *DHRS2* and HIV-1 mRNA expression follow similar expression kinetics. Similarly, the antiviral factors *GBP2* and *GBP5* are located downstream of individual *LTR12C* elements, suggesting potential *cis*-regulation of the expression of these ISGs by those endogenous retrovirus elements[40]. Expression of *GBP5* was upregulated upon Panobinostat treatment in the T_{EM} subset in primary $CD4^+$ T-cells and J1.1 T-cells. Reactivation of HIV-1 transcription potentially triggers *GBP2* expression, as *GBP2* has been reported to be induced by acute HIV-1 infection in primary $CD4^+$ T-cells[40]. This feed-forward loop might explain the lack of HDACi-induced *GBP2* expression in the primary $CD4^+$ T-cell data, where HIV-1 expression is absent in the majority of cells. Overall, we show that HDAC inhibitors induce the expression of cellular genes that are under the control of LTR12 elements, thereby indirectly supporting existing data that HDAC inhibitors trigger the expression of endogenous retroviruses from the LTR12 family[69].

In PLHIV with fully suppressed viremia, 10^2 per 10^6 circulating $CD4^+$ T-cells harbour intact, reactivatable proviral DNA[70–72]. Determination of this frequency is based on amplification of near full-length proviral genomes, assuming their intactness, and/or detection of HIV-1 RNA positivity as direct evidence of reactivability of respective proviruses using RNA flow/FISH[22]. Our data showing a frequency of $CD4^+$ T-cells with detectable HIV-1 transcription of $200/10^6$ in the context of mock treatment is consistent with these reports. The low increase of the prevalence of HIV-1 RNA-positive cells upon IL-2/PHA and HDACi treatment is reminiscent of similar observations obtained in the context of PMA/ionomycin treatment[73],

bioRxiv preprint doi: https://doi.org/10.1101/2020.05.04.075119; this version posted June 4, 2023. The copyright holder for this preprint (which was not certified by peer review) is the author/funder, who has granted bioRxiv a license to display the preprint in perpetuity. It is made available under aCC-BY-NC 4.0 International license.

suggesting that a substantial proportion of proviruses are refractory to stimulation. In agreement with other studies[74], our data argue against the existence of a distinct cellular marker that is specifically expressed in HIV-1-positive cells. A limitation of our study is the lack of identification of HIV-1 RNA-negative, though provirus-positive cells, probably explaining our inability to confirm reports of a skewed transcriptional milieu in HIV-1-positive cells that favours HIV-1 silencing, cell survival and cell proliferation, including inhibition of death receptor signalling, necroptosis signalling and antiproliferative Gα12/13 signalling[75]. A study analysing the combined transcriptional profile of $CD4^+$ T-cells from both viremic and aviremic individuals reported that most HIV-1 RNA-positive $CD4^+$ T cells were GZMB-positive cytotoxic effector memory Th1s, some of them expressing *SERPINB9* resulting being shielded from killing by cytotoxic $CD8^+$ T cells [76]. While these studies provide elegant rationales for the overall persistence of HIV-1-positive cells, corresponding data were based on datasets that included $CD4^+$ T-cells harbouring non-reactivatable proviruses and acutely infected cells, respectively. Our study is restricted to $CD4^+$ T-cells carrying transcriptionally active proviruses, which are the most relevant ones to target in an elimination approach, in the context of full virus suppression, thereby excluding to a great extent acute, non-latent infection. Under these conditions, we identified specific genes being differentially expressed in HIV-1 RNA-positive versus cells in which HIV-1 RNA was undetectable. *PSRC1*/*DDA3* has been initially identified as a down-stream target of p53 and is involved in microtubule dynamics [77,78], but has not been yet associated with infectious diseases or HIV-1 specifically. HES6 is a transcription (co-) factor that has been reported to be overexpressed in multiple cancers [79,80], but little is known about its exact functionality or implication for infectious diseases or HIV-1 replication. *PLCD1* encodes for an enzyme of the phospholipase C family and catalyses the hydrolysis of PIP2 into the second messenger DAG and IP3, thereby exerting multiple effects in intracellular signal transduction (reviewed in [81]. Interestingly, another member of the phospholipase family has been reported to modulate HIV-1 replication [82]. Future studies will need to uncover if expression of these genes is cause or consequence of concomitant hIV-1 mRNA expression, and characterise their role in the context of HIV-1 latency reversal.

bioRxiv preprint doi: https://doi.org/10.1101/2020.05.04.075119; this version posted June 4, 2023. The copyright holder for this preprint (which was not certified by peer review) is the author/funder, who has granted bioRxiv a license to display the preprint in perpetuity. It is made available under aCC-BY-NC 4.0 International license.

MATERIAL AND METHODS

Cell lines and primary cells

HEK293T cells were maintained in Dulbecco's modified Eagle's medium (DMEM) supplemented with 10% heat-inactivated fetal calf serum, 100 IU/ml Penicillin/Streptomycin (Thermo Fisher Scientific) and 2 mM L-Glutamine (Thermo Fisher Scientific) in a 5% CO_2 atmosphere at 37°C. Jurkat and J1.1 T-cells were obtained from the NIH AIDS Reagents Program and cultivated in RPMI 1640 supplemented with 10% heat-inactivated fetal calf serum, 100 IU/ml Penicillin/Streptomycin (Thermo Fisher Scientific) and 2 mM L-Glutamine (Thermo Fisher Scientific) in a 5% CO_2 atmosphere at 37 °C.

Withdrawal of blood samples from healthy human donors and cell isolation were conducted with approval of the local ethics committee (Ethical review committee of Charité Berlin, vote EA4/167/19). Withdrawal of blood samples from aviremic, HIV-1-infected individuals and cell isolation were conducted with approval of the local ethics committee (Ethical review committee of Charité Berlin, votes EA2/105/05 and EA2/024/21) in the context of the HIV-1 Seroconverter Study of the Robert-Koch-Institute[83]. Available clinical information is indicated in Supplementary Table 1. Human $CD4^+$ T-cells were isolated using the EasySep Direct Human $CD4^+$ T-Cell Isolation Kit (STEMCELL Technologies). $CD4^+$ T-cells were cultured at 1×10^6/ml in RPMI 1640 containing 10% heat-inactivated fetal calf serum (Sigma-Aldrich), 100 IU/ml penicillin/streptomycin (Thermo Fisher Scientific), 2 mM L-Glutamine (Thermo Fisher Scientific), 1% MEM non-essential amino acids (Thermo Fisher Scientific) and 1 mM sodium pyruvate (Thermo Fisher Scientific).

Reagents and inhibitors

bioRxiv preprint doi: https://doi.org/10.1101/2020.05.04.075119; this version posted June 4, 2023. The copyright holder for this preprint (which was not certified by peer review) is the author/funder, who has granted bioRxiv a license to display the preprint in perpetuity. It is made available under aCC-BY-NC 4.0 International license.

The following reagents were used: Bryostatin I (#B7431; Sigma Aldrich), CEFX Ultra SuperStim Pool (#PM-CEFX-1, JPT), IFN-□2a (Roferon; Roche), IL-2 (#11011456001; Merck), Panobinostat (#13280; Cayman Chemical), PHA (#R30852801; Thermo Scientific), Vorinostat/SAHA (#ab144480; abcam).

Treatment of CD4⁺ T-cells for single cell RNA-sequencing

CD4⁺ T-cells were mock-treated (0.05% DMSO) or treated with Vorinostat (500 nM), Panobinostat (50 nM) or IL-2 (20 IU/ml) and PHA (1 □g/ml) for 48 hours before subjecting them to the single cell RNA-sequencing pipeline. J1.1 T-cells were treated with 1.6% DMSO (DMSO I), 16000 nM Vorinostat, 0.2% DMSO (DMSO II) or 200 nM Panobinostat for 40 hours before subjecting them to single cell RNA-sequencing.

Single cell RNA-sequencing

Single cell RNA-Seq libraries were prepared with the 10x Genomics platform using the Chromium Next GEM Single Cell 3' Reagent Kits v.3.1 following manufacturer's instructions. Quality control of the libraries were performed with the KAPA Library Quantification Kit and Agilent TapeStation. Libraries were sequenced on a HiSeq4000 using the following sequencing mode: read 1: 28 bp, read 2: 91-100 bp, Index i7: 8 bp. The libraries were sequenced to reach ~20 000 reads per cell.

Single cell RNA-sequencing data analysis

FASTQ files from the sequencing protocol were processed using the Cell Ranger pipeline v 3.1.0 (10X Genomics) and further analysed using the Seurat v3.1.4 package[84] in R v3.6 (R Core Team, 2017). Reads from cells isolated from PLHIV were aligned to the human genome (GRCh38), while reads from J1.1 T-cells were aligned to a custom reference consisting of the genomic HIV-1 RNA (LAV-1, GenBank: K02013.1) appended to GRCh38 to allow for capture of viral RNAs. The data was processed using the SCTransform workflow as outlined by the Seurat developers. Cells were clustered using Louvain clustering in a UMAP projection. For

bioRxiv preprint doi: https://doi.org/10.1101/2020.05.04.075119; this version posted June 4, 2023. The copyright holder for this preprint (which was not certified by peer review) is the author/funder, who has granted bioRxiv a license to display the preprint in perpetuity. It is made available under aCC-BY-NC 4.0 International license.

the CD4$^+$ T-cells from PLHIV, T-cell subsets were identified based on marker gene expression: T_N cells (CD3D$^+$, CD8A$^-$, CCR7$^+$, S100A4^{low})[25], T_{CM} cells (CD3D$^+$, CD8A$^-$, CCR7^{low}, S100A4^{int}, CD62L^{high}, GZMA$^-$)[85] T_{TM} cells (CD3D$^+$, CD8A$^-$, CCR7^{low}, S100A4^{high}, CD62L^{low}, GZMA$^+$, GZMB$^-$, GZMH$^-$, PRF1$^-$, GNLY$^+$)[4,86,87], T_{EM} cells (CD3D$^+$, CD8A$^-$, CCR7$^-$, S100A4^{high}, GZMA$^+$, GZMB$^+$, GZMH$^+$, PRF1$^+$ GNLY$^+$)[88], T_{EMRA} cells (CD3D$^+$, CD8A$^-$, CCR7$^-$, S100A4^{high}, GZMA$^+$, GZMB^{high}, GZMH$^+$, PRF1^{high}, GNLY^{high}, CCL4$^+$)[26,89], T_{REG} cells (CD3D$^+$, CD8A$^-$, CCR7^{low}, S100A4^{high}, FOXP3$^+$, IL2RA$^+$, CTLA4$^+$)[26,90], T_{EX} cells (CD3D$^+$, CD8A$^-$, CCR7$^-$, GZMB$^+$, PDCD1$^+$, LAG3$^+$)[91]. All utilized code is deposited at https://github.com/GoffinetLab/HIV_scRNAseq-CD4-LRA-study. To visualize sequencing coverage of the viral genome in J1.1 T-cells, viral reads were extracted from the bam files of the CellRanger output. These were converted to bigwig files and visualised on tracks using bamCoverage (setting –normalizeUsing RPGC) and pyGenomeTracks from deeptools [92].

Principal component analysis (PCA)

PCA was performed with the average expression values of all genes with detectable expression levels of mock-, Vorinostat- and Panobinostat-treated samples. Singular value decomposition (SVD) with imputations was used for calculation of the principal components using ClustVis (https://biit.cs.ut.ee/clustvis/)[93].

Differentially expressed genes and pathway analysis

DEGs between individual treatments were identified using the 10x Genomics Loupe Browser (v. 5.0.1.); p-values were adjusted using the Benjamini-Hochberg correction for multiple testing. Pathway analysis was performed with the list of DEGs harbouring p-values <0.05, gene set enrichment analysis (GSEA) was performed using the Pathway Panther database[94–96]. The results are described using the Normalised Enrichment Ratio (NER), the enrichment ratio indicates the degree of overrepresentation of a given gene set in the list of DEGs and is normalised to take different gene set sizes into account.

bioRxiv preprint doi: https://doi.org/10.1101/2020.05.04.075119; this version posted June 4, 2023. The copyright holder for this preprint (which was not certified by peer review) is the author/funder, who has granted bioRxiv a license to display the preprint in perpetuity. It is made available under aCC-BY-NC 4.0 International license.

To identify genes that are specifically expressed in J1.1 T-cells presenting high expression of HIV-1 RNA, we defined HIV-1-high cells above the 75th percentile of HIV-1 expression for each treatment. For the DMSO controls, HIV-1-high cells were compared to cells with no detectable HIV-1 expression (HIV-1-negative). For the LRA treatments, HIV-1-low cells were defined as cells exhibiting HIV-1 RNA expression below the 90th percentile of HIV-1 expression in the matched DMSO control, representing the majority of cells showing basal and DMSO-induced HIV-1 reactivation. The HIV-1-high and HIV-1-low cells for each LRA treatment were then compared to identify DEGs between these groups. The individual groups of cells (HIV-1-high, -low and -negative) are depicted in Fig. 4A for clarity.

To identify DEGs between HIV-1 RNA-positive and -negative cells in the primary $CD4^+$ dataset, we used two different approaches. Firstly, we used the Seurat FindMarkers function to identify DEGs between the 36 HIV-1 RNA-positive cells and all other cells in the dataset. In a second approach we aimed at comparing groups consisting of identical numbers of cells of identical cell subset and treatment. To this end, we randomly selected, from the total pool of HIV-1 RNA-negative cells, a group of cells with the identical subset and treatment distribution as is represented in the HIV-1 RNA-positive cell group, yielding 36 subset- and treatment-matched, HIV-1-negative cells, in 5,000 bootstrapped iterations. For each iteration, we performed analysis of DEGs using the FindMarkers function from Seurat. Fold changes were averaged across all 5,000 iterations and a Chi-squared test (with Bonferroni correction) was used to identify DEGs (p-value < 0.05) in all iterations at a rate greater than chance (probability of 50%).

Transcription factor activity analysis

Transcription factor activity analysis was performed using the dorothea R package following the guidelines for processing single cell RNA-seq data [97,98], with the following exception. The run_viper function from dorothea was altered to use the top 40,000 most variable genes, as

bioRxiv preprint doi: https://doi.org/10.1101/2020.05.04.075119; this version posted June 4, 2023. The copyright holder for this preprint (which was not certified by peer review) is the author/funder, who has granted bioRxiv a license to display the preprint in perpetuity. It is made available under aCC-BY-NC 4.0 International license.

determined by the FindVariableFeatures function from Seurat. Utilised code is available at https://github.com/GoffinetLab/HIV_scRNAseq-CD4-LRA-study.

Module scores

The IFN signalling pathway (R-HSA-913531) and TCR signalling pathway (R-HSA-202403) gene sets from the Reactome database[99] were retrieved from the Molecular Signatures Database (MSigDB)[100]. Cells were scored based on their expression of these genes using the AddModuleScore function in Seurat. They are referred to as the IFN signalling module and T-cell activation module scores as the pathways include genes canonically involved in response to IFN signalling and TCR-mediated T-cell activation, respectively.

HIV-1 RNA correlation analysis

To identify which genes whose expression correlates with viral RNA expression in the J1.1 cells, DEGs between HIV-1-high and HIV-1-low groups were calculated as described above and the Seurat objects were then converted to SingleCellExperiment objects[101] in order to perform pairwise correlations of these genes with HIV-1 RNA expression using the correlatePairs function from the scran package[102]. The resulting p-values were corrected using a stringent Bonferroni correction.

Identification of HIV-1 RNA in primary CD4⁺ T-cells

Since HIV-1 sequences are highly diverse, we aligned all single-cell data to about 14,000 available HIV-1 genome sequences in order to increase the probabilities for proper mappings. Full-genome HIV-1-specific sequences were obtained from the Los Alamos HIV Database (http://www.hiv.lanl.gov/). The sequences were then split in subsets, with 100 each in one fasta file. This fasta file was then used to create a hisat2 [doi: 10.1038/s41587-019-0201-4] index

bioRxiv preprint doi: https://doi.org/10.1101/2020.05.04.075119; this version posted June 4, 2023. The copyright holder for this preprint (which was not certified by peer review) is the author/funder, who has granted bioRxiv a license to display the preprint in perpetuity. It is made available under aCC-BY-NC 4.0 International license.

and then the read2 files of all single-cell experiments were aligned using the following parameters: hisat2 -p 6 --all --secondary --mp 2,1 -x [index file] --no-unal --pen-noncansplice 0 --pen-noncanintronlen G,0,0 --pen-canintronlen G,0,0 -U [read file]. Reference sequences were then clustered by the number of reads that would align to reads obtained from CD4+ T-cells using pheatmap (https://cran.r-project.org/web/packages/pheatmap/index.html). Some of the clusters contained sequences with artifactually high numbers of aligned reads. For each donor, we identified a specific cluster, and took the top 30 sequences from that cluster, i.e. the ones with the most aligned reads. Alignments were manually inspected for all 30 sequences, and about 20 sequences per donor selected for final alignments (**Supplementary Table 3**). All reads aligning to these sequences were then estimated as "true positive", i.e. coming from the actual virus in the respective donor. Viral genome coverage was visualised using bamCoverage and pyGenomeTracks [92] as mentioned above.

Flow cytometry

PBS-washed cells were immunostained for individual surface proteins using the following antibodies: anti-CCR5/CD195 (#555992; BD Biosciences), anti-CCR7/CD197 (#552176; BD Biosciences), anti-CD3-FITC (#561807; BD Biosciences), anti-CD4-APC (#555349; BD Biosciences), anti-CD25 (#340929; BD Biosciences), anti-CD45RA (#335039; BD Biosciences), anti-CD45RO (#340438; BD Biosciences), anti-CD62L (#304804; Biolegend), anti-CD69 (#340560; BD Biosciences), anti-CXCR4/CD184 (#555976; BD Biosciences), anti-HLA-DR (#556643, BD Biosciences), anti-IL7R, anti-PD-1/CD279-PE (#21272794; ImmunoTools) and anti-TIM-3/CD366-FITC (#345022; Biolegend). Cell viability was analysed using the Dead Cell Apoptosis Kit for Flow Cytometry from Invivogen (#V13242), with early apoptotic cells scoring Annexin V-positive and late apoptotic cells scoring Annexin V- and propidium iodide (PI)-positive. For intracellular immunostaining, PBS-washed cells were PFA-fixed for 90 minutes and immunostained with the following antibodies diluted in 0.1% Triton X-100 in PBS: anti-HIV-1-core-antigen-FITC (mouse, 1:200 dilution; KC57; Beckman

bioRxiv preprint doi: https://doi.org/10.1101/2020.05.04.075119; this version posted June 4, 2023. The copyright holder for this preprint (which was not certified by peer review) is the author/funder, who has granted bioRxiv a license to display the preprint in perpetuity. It is made available under aCC-BY-NC 4.0 International license.

Coulter), rabbit-anti-human-MX1/2 (#sc-166412; Santa Cruz Biotechnology). A goat-anti-rabbit IgG conjugated to Alexa Fluor 647 (#A27040; Thermo Fisher) was used as a secondary antibody. Data acquisition and analysis was conducted using a FACS Celesta device (Becton Dickinson, Franklin Lakes, New Jersey, USA) with FlowJo (v.10.7.1).

T-cell activation assays

$CD4^+$ T-cells were isolated from healthy donors and pre-incubated with Vorinostat (500 nM), Panobinostat (50 nM), or left mock-treated (0.05% DMSO) for 16 hours followed by stimulation with a peptide pool of a broad range of HLA-subtypes and infectious agents (CEFX Ultra SuperStim Pool; JPT) (1 µg/ml) and 1 □g/ml mouse-anti-human CD28 antibody (#556620; BD Biosciences), or IL-2 (20 IU/ml) and PHA (1 µg/ml). T-cell activation and exhaustion was quantified by flow cytometry 48 hours post-stimulation.

HIV-1 reactivation assays in J1.1 T-cells

J1.1 cells were PBS-washed, resuspended in fresh cell culture RPMI and incubated with Vorinostat, Panobinostat, Bryostatin or DMSO at the indicated concentrations. In some assays, J1.1 cells were pre-incubated with IFN-α2a (Roferon) for 24 hours before addition of the LRA. Samples were collected at indicated time points and subjected to RT-Q-PCR or flow cytometric analysis.

Quantitative RT-Q-PCR

RNA extraction was followed by cDNA synthesis (NEB, Invitrogen). Quantification of relative mRNA levels was performed with the LightCycler 480 Instrument II (Roche) using Taq-Man PCR technology. For human *IFIT1* and *MX2*, a premade primer-probe kit was purchased from Applied Biosystems (Assay ID: Hs01911452_s1; Hs01550813_m1; respectively. Relative mRNA levels were determined using the ΔΔCt method using human *RNASEP* (Applied

bioRxiv preprint doi: https://doi.org/10.1101/2020.05.04.075119; this version posted June 4, 2023. The copyright holder for this preprint (which was not certified by peer review) is the author/funder, who has granted bioRxiv a license to display the preprint in perpetuity. It is made available under aCC-BY-NC 4.0 International license.

Biosystems) as internal reference. Data analysis was performed using LightCycler Software 4.1 (Roche).

Data presentation and statistical analysis

Graphs and figures were generated using Graphpad Prism 9 (v.9.1.2.) and Adobe Illustrator 2021. Heatmaps were generated using the ClustVis web tool (https://biit.cs.ut.ee/clustvis/) with unit variance scaling for rows[93]. If not otherwise stated, bars represent the mean of the indicated number of experiments and error bars indicate the S.E.M. Statistical significance for paired data sets were tested using Graphpad Prism 9 (v.9.1.2.) and paired student's t-testing, symbols indicate the obtained p-values: * (p-value from 0.01 - 0.05), ** (p-value from 0.01 - 0.001) and *** (p-value < 0.001) or n.s. (p-value ≥ 0.05).

Data availability

The single cell RNA-sequencing data will be deposited at the Gene Expression Omnibus (GEO) database (accession number #).

Acknowledgments

We thank the individuals with HIV-1 who agreed to participate in the Seroconverter Study and provide his blood for research. We thank the NIH AIDS Research & Reference Reagent

bioRxiv preprint doi: https://doi.org/10.1101/2020.05.04.075119; this version posted June 4, 2023. The copyright holder for this preprint (which was not certified by peer review) is the author/funder, who has granted bioRxiv a license to display the preprint in perpetuity. It is made available under aCC-BY-NC 4.0 International license.

Program for providing essential reagents. We thank the Genomics Platform of the Berlin Institute of Health for next-generation sequencing. This work was supported by funding to C.G. by Berlin Institute of Health (BIH); by Hector Foundation, project M2101; by DFG priority program 1923 "Innate Sensing and Restriction of Retroviruses," grant GO2153/4); by DZIF, TTU HIV, grant 04.820 to C.G. We thank Christian Drosten for constant support. J.K. is supported by the Center of Infection Biology and Immunity (ZIBI) and Charité PhD Program.

Author contributions

JK, JF, TS, JJ performed experiments.

JK, DP, EW, JF, TS, CF, SNV, MS analysed data.

UK, BGB, KM, NB, LL, AT provided essential resources.

AT, SS, NB, ML, CG supervised.

CG acquired funding and managed the project.

JK, DP, CG wrote the manuscript.

Declaration of conflicts of interest

None.

bioRxiv preprint doi: https://doi.org/10.1101/2020.05.04.075119; this version posted June 4, 2023. The copyright holder for this preprint (which was not certified by peer review) is the author/funder, who has granted bioRxiv a license to display the preprint in perpetuity. It is made available under aCC-BY-NC 4.0 International license.

FIGURES

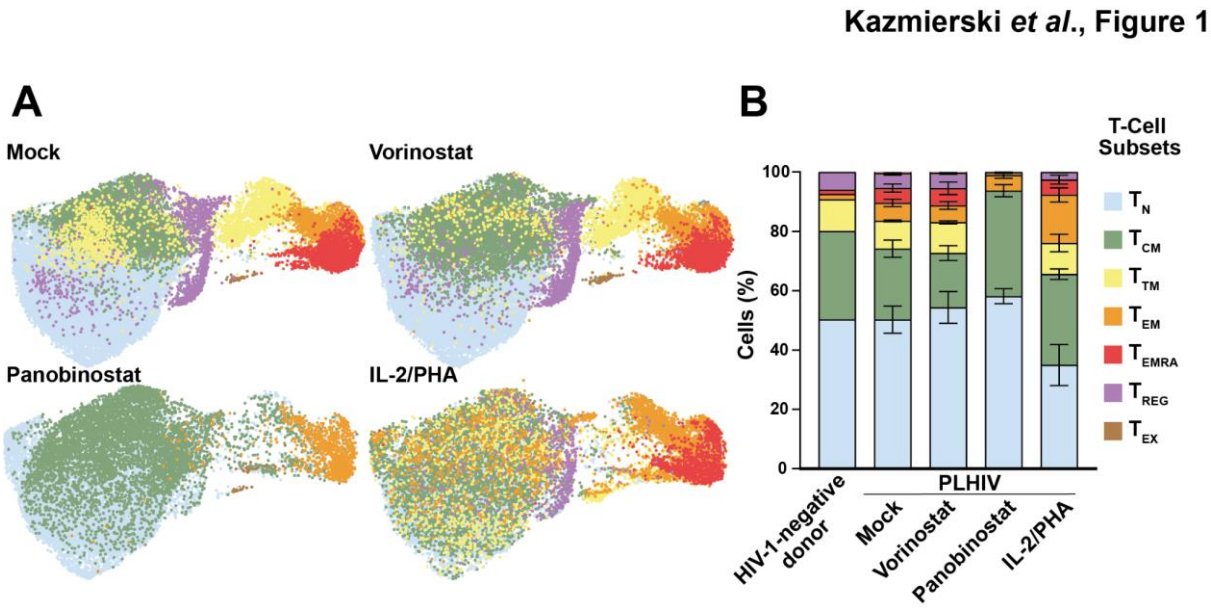

Figure 1. Panobinostat treatment modulates expression of CD4⁺ T-cell subset-specific markers

(**A**) Combined UMAP plot of CD4⁺ T-cell cultures from three PLHIV, separated by treatment and coloured by T-cell subset.

(**B**) Percentages of the indicated CD4⁺ T-cell subsets.

bioRxiv preprint doi: https://doi.org/10.1101/2020.05.04.075119; this version posted June 4, 2023. The copyright holder for this preprint (which was not certified by peer review) is the author/funder, who has granted bioRxiv a license to display the preprint in perpetuity. It is made available under aCC-BY-NC 4.0 International license.

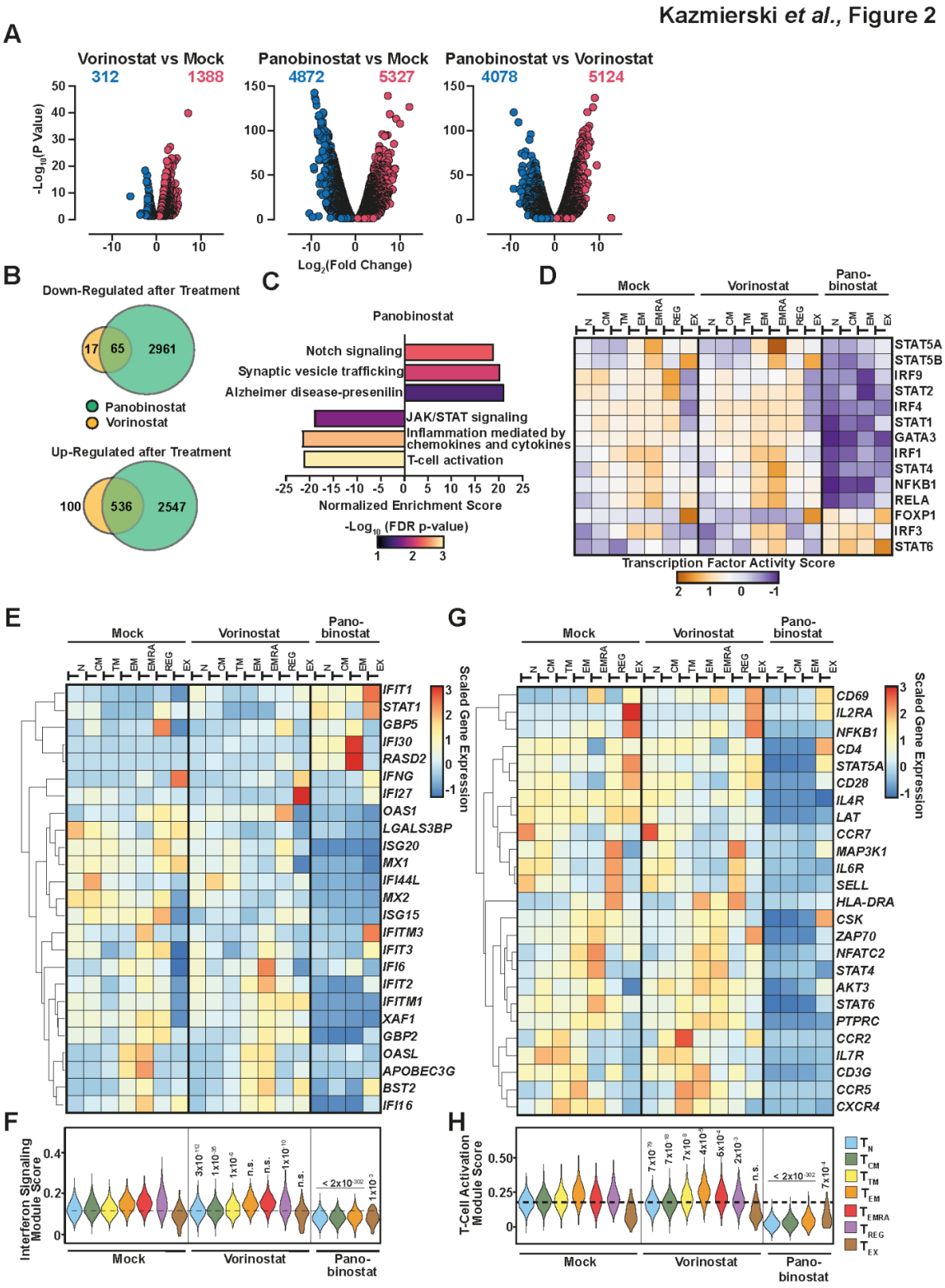

Figure 2. Panobinostat treatment induces broad transcriptional down-modulation of genes involved in T-cell signalling and innate immunity

bioRxiv preprint doi: https://doi.org/10.1101/2020.05.04.075119; this version posted June 4, 2023. The copyright holder for this preprint (which was not certified by peer review) is the author/funder, who has granted bioRxiv a license to display the preprint in perpetuity. It is made available under aCC-BY-NC 4.0 International license.

(**A**) Volcano plots showing DEGs with a p-value < 0.05.

(**B**) Overlap of genes significantly up- or down-regulated (p-value < 0.05, fold change > 2) in Vorinostat and Panobinostat-treated samples compared to mock treatment.

(**C**) Pathway analysis of DEGs (p-value < 0.05) after Panobinostat treatment. Shown is the Normalised Enrichment Ration (NER), representing the degree of overrepresentation of a given gene set in the DEG list. Colours indicate the $-Log_{10}$(FDR p-value).

(**D**) Transcription factor activity analysis of selected transcription factors in the indicated T-cell subsets.

(**E**) Heatmap showing scaled average expression of selected ISGs in the indicated T-cell subsets. Genes are ordered based on correlation, clustering is indicated with lines on the left.

(**F**) Average IFN signalling module score in the indicated T-cell subsets. Dashed line shows the average module score of mock-treated T_N-cells. Numbers indicate the p-value calculated using Wilcoxon signed-rank testing for each subset from the LRA-treated samples compared to the same subset of the mock-treated samples.

(**G**) Heatmap showing scaled average expression of selected genes required for T-cell-mediated immunity in the indicated T-cell subsets. Genes are ordered based on correlation, clustering is indicated with lines on the left.

(**H**) Average T-cell activation module score in the indicated T-cell subsets. Dashed line shows the average module score of mock-treated T_N-cells. Numbers indicate the p-value calculated using Wilcoxon signed-rank testing for each subset from the LRA-treated samples compared to the same subset of the mock-treated samples.

bioRxiv preprint doi: https://doi.org/10.1101/2020.05.04.075119; this version posted June 4, 2023. The copyright holder for this preprint (which was not certified by peer review) is the author/funder, who has granted bioRxiv a license to display the preprint in perpetuity. It is made available under aCC-BY-NC 4.0 International license.

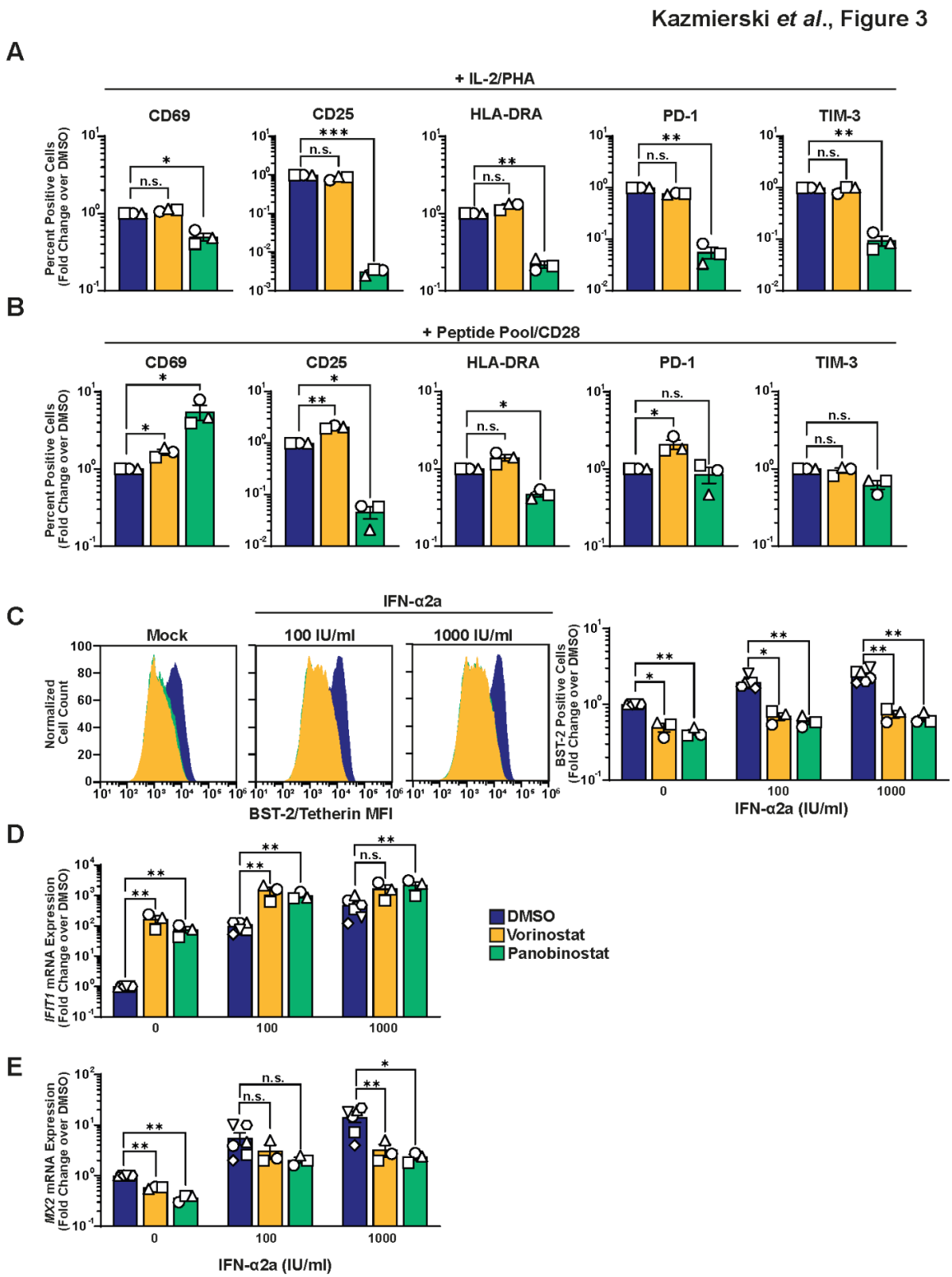

Figure 3. HDAC inhibition imposes a block to CD4⁺ T-cell activation and type I IFN signalling

bioRxiv preprint doi: https://doi.org/10.1101/2020.05.04.075119; this version posted June 4, 2023. The copyright holder for this preprint (which was not certified by peer review) is the author/funder, who has granted bioRxiv a license to display the preprint in perpetuity. It is made available under aCC-BY-NC 4.0 International license.

$CD4^+$ T-cells from HIV-1-negative donors were either pretreated with 0.5% DMSO, 500 nM Vorinostat or 50 nM Panobinostat for 16 hours, followed by:

(**A**) Stimulation with a pool of peptide epitopes and anti-CD28 antibody for 48 hours

(**B**) Stimulation with IL-2/PHA for 48 hours

followed by analysis of CD69, CD25, HLA-DR, TIM-3 and PD-1 cell surface expression by flow cytometry. Shown are data from cells from three donors.

$CD4^+$ T-cells from HIV-1-negative donors were co-treated with 0.5% DMSO, 8000 nM Vorinostat or 50 nM Panobinostat in combination with increasing concentrations of IFN-α2a for 48 hours before analysing:

(**C**) BST2 cell surface levels by flow cytometry. Shown are representative histograms from one experiment (left panel) and quantification from experiments with cells from three donors.

(**D**) *IFIT1* mRNA expression by RT-Q-PCR. Shown are data from cells from 3-6 donors.

(**E**) *MX2* mRNA expression by RT-Q-PCR. Shown are data from cells from 3-6 donors.

bioRxiv preprint doi: https://doi.org/10.1101/2020.05.04.075119; this version posted June 4, 2023. The copyright holder for this preprint (which was not certified by peer review) is the author/funder, who has granted bioRxiv a license to display the preprint in perpetuity. It is made available under aCC-BY-NC 4.0 International license.

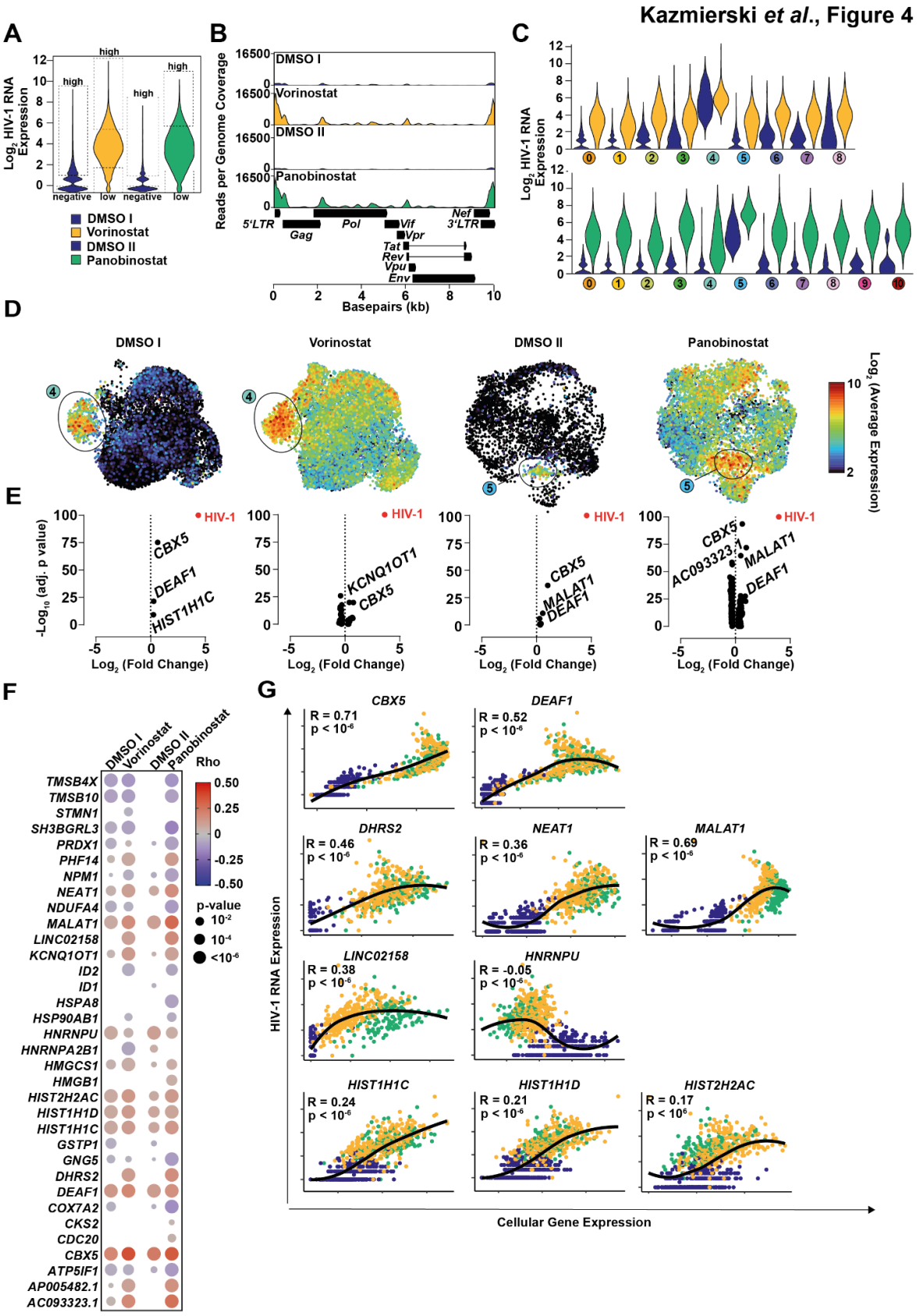

bioRxiv preprint doi: https://doi.org/10.1101/2020.05.04.075119; this version posted June 4, 2023. The copyright holder for this preprint (which was not certified by peer review) is the author/funder, who has granted bioRxiv a license to display the preprint in perpetuity. It is made available under aCC-BY-NC 4.0 International license.

Figure 4. HIV-1 RNA abundance correlates with specific cellular gene expression in J1.1 T-cells

(**A**) Violin plot showing HIV-1 RNA expression per cell in J1.1 T-cells after indicated treatments (1.6% DMSO (DMSO I); Vorinostat (16 µM); 0.2% DMSO (DMSO II); Panobinostat (200 nM). Boxes indicate HIV-1-high, -low, and -negative cells of the different treatments that are used for differential gene expression analysis.

(**B**) Coverage plot of HIV-1-specific reads aligned to the HIV-1 LAI genomic RNA.

(**C**) Violin plot showing HIV-1 RNA expression per cell in the individual clusters after Vorinostat, Panobinostat or DMSO treatment.

(**D**) UMAP plots of individually treated J1.1 cells coloured by HIV-1 RNA expression. Highlighted are the clusters with high HIV-1 RNA abundance.

(**E**) Differentially expressed gene analysis of HIV-1-RNA-high expressing cells compared to HIV-1-RNA-low expressing cells as defined by the 75th or 90th percentile of HIV-1 RNA expression in LRA-treated or DMSO-treated samples, respectively. The complete list of DEGs is provided in Supplementary Table 3.

(**F**) Dotplots visualising the correlation analysis of HIV-1 RNA expression with expression of cellular genes that were most differentially expressed among HIV-high vs HIV-low J1.1 T-cells (identified in E). Only statistically significant correlations are shown ($p < 0.05$). The dot size corresponds to the p-value and the colour intensity with Spearman's rank correlation coefficient (Rho).

(**G**) Correlation plots for expression of selected cellular genes with expression of HIV-1 RNA after indicated treatments. The dots correspond to the individual expression levels of binned cells (100 cells/bin).

bioRxiv preprint doi: https://doi.org/10.1101/2020.05.04.075119; this version posted June 4, 2023. The copyright holder for this preprint (which was not certified by peer review) is the author/funder, who has granted bioRxiv a license to display the preprint in perpetuity. It is made available under aCC-BY-NC 4.0 International license.

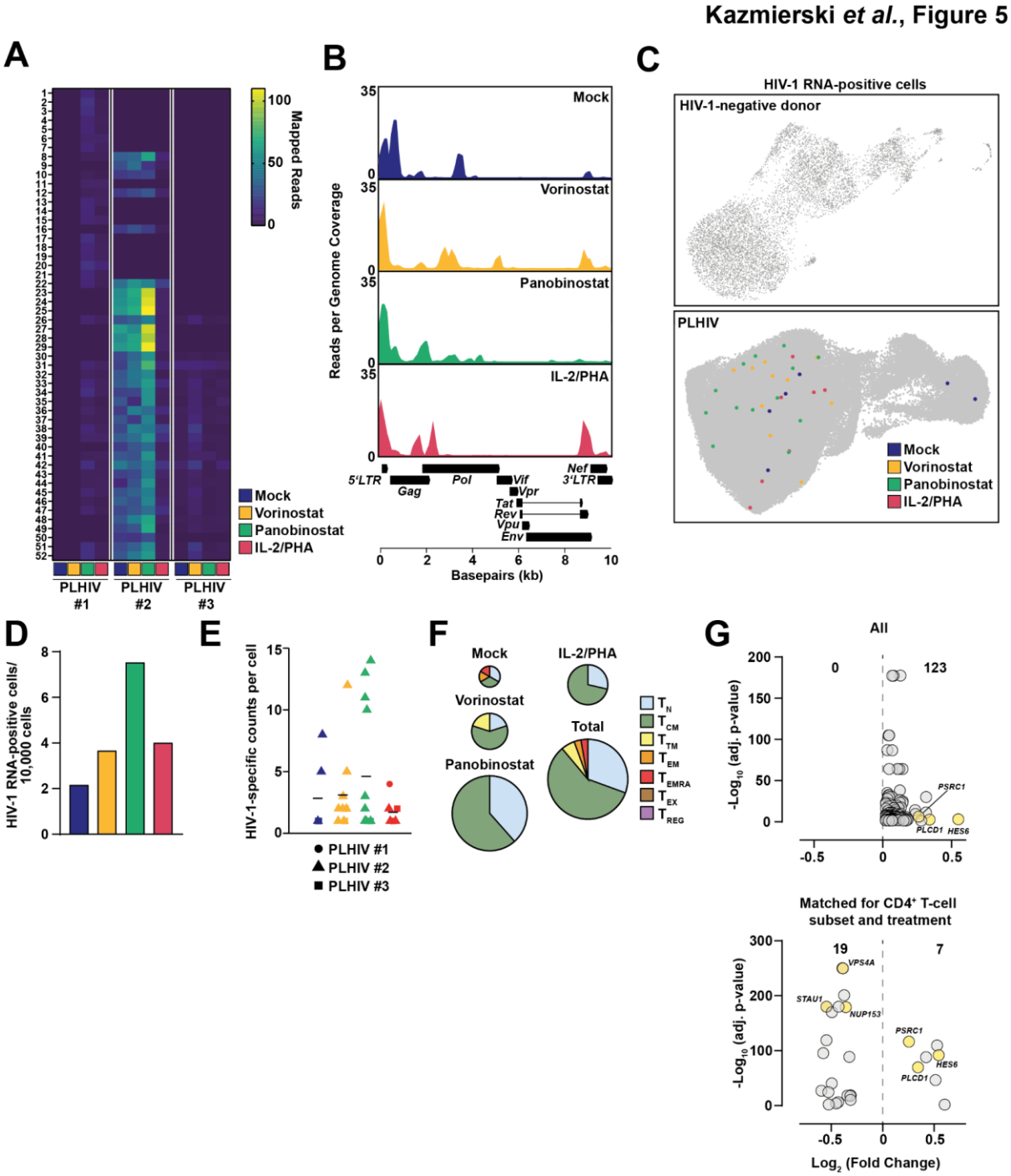

Figure 5. Detection of HIV-1 RNA in CD4⁺ T-cells from PLHIV and associating cellular gene expression

(**A**) Heatmap showing the number of reads specifically mapping to HIV-1 isolate sequences (1-52) from the individual samples. HIV-1 isolate sequences were derived from the Los Alamos database, only sequences that showed specific binding were used.

bioRxiv preprint doi: https://doi.org/10.1101/2020.05.04.075119; this version posted June 4, 2023. The copyright holder for this preprint (which was not certified by peer review) is the author/funder, who has granted bioRxiv a license to display the preprint in perpetuity. It is made available under aCC-BY-NC 4.0 International license.

(**B**) Coverage plot of HIV-1-specific reads aligned with the HIV-1 genomic RNA.

(**C**) UMAP showing HIV-1-positive cells coloured by treatment in $CD4^+$ T-cells from an HIV-1-negative donor and three PLHIV.

(**D**) Quantification of HIV-1 RNA-positive cells/10,000 cells analysed for the individual treatments.

(**E**) Numbers of HIV-1 reads per cell of cells displaying at least one HIV-1 read

(**F**) Pie charts showing the T-cell subtypes of HIV-1 RNA-positive cells.

(**G**) DEG analysis of HIV-1-RNA-positive vs HIV-1-RNA-negative cells calculated based on all cells (left) or by comparing all HIV-1 RNA-positive cells to 36 cell type and treatment matched, randomly sampled HIV-1 RNA negative cells over 5000 sampling iterations. Indicated are the average fold changes over all iterations. Genes with an adjusted p-value < 0.05 are shown.

bioRxiv preprint doi: https://doi.org/10.1101/2020.05.04.075119; this version posted June 4, 2023. The copyright holder for this preprint (which was not certified by peer review) is the author/funder, who has granted bioRxiv a license to display the preprint in perpetuity. It is made available under aCC-BY-NC 4.0 International license.

SUPPLEMENTARY MATERIALS

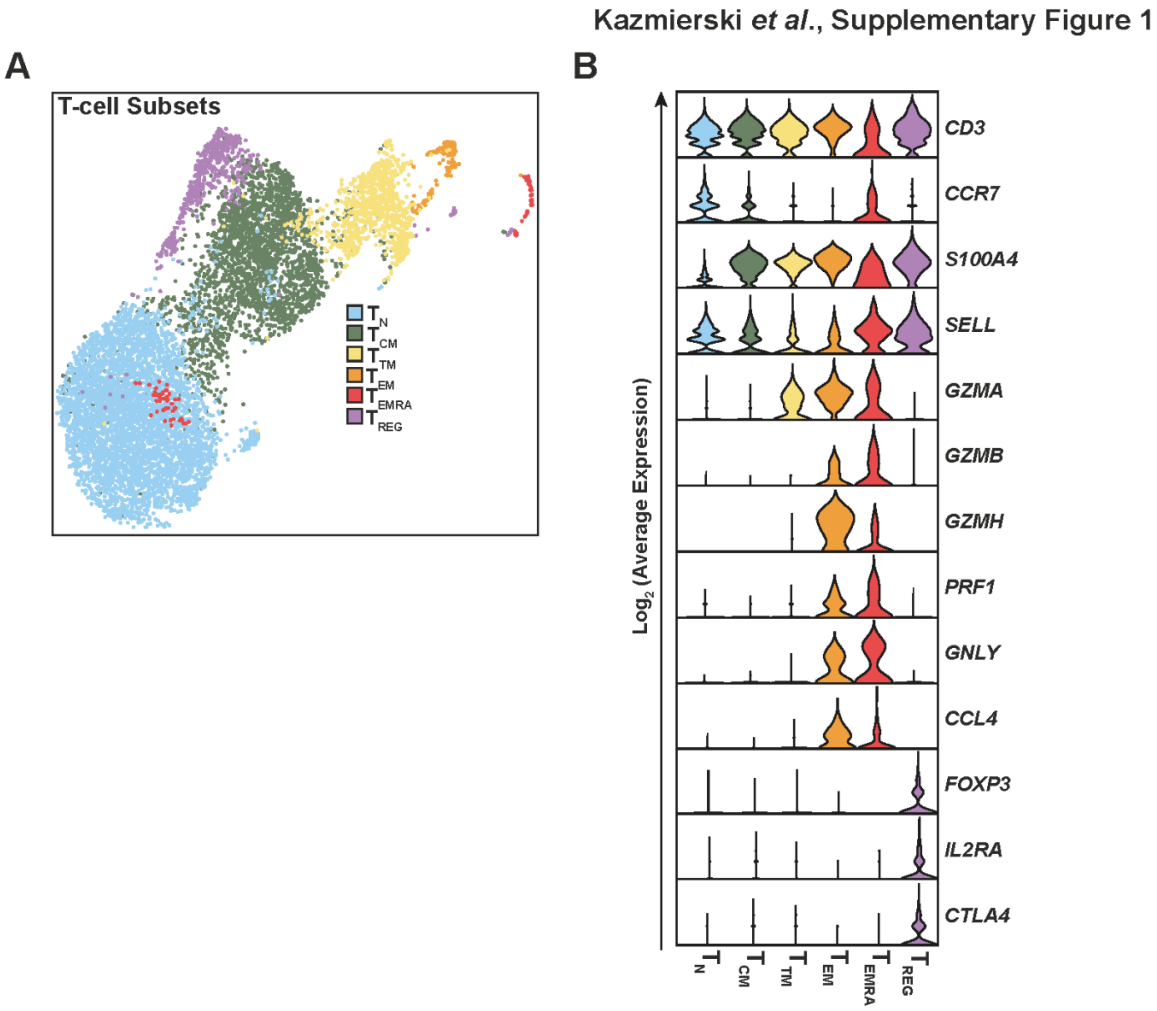

Supplementary Figure 1. Identification of T-cell subsets in CD4⁺ T-cells isolated from an HIV-1-negative donor

(**A**) UMAP plot showing T-cell subsets that were identified based on specific marker gene expression: Naïve (T_N), Central Memory (T_{CM}), Transitory Memory (T_{TM}), Effector Memory (T_{EM}), Effector Memory Cells Re-Expressing CD45RA (T_{EMRA}) and Regulatory (T_{REG}).

(**B**) Violin plot showing T-cell subset specific marker gene expression in the identified T-cell subsets.

bioRxiv preprint doi: https://doi.org/10.1101/2020.05.04.075119; this version posted June 4, 2023. The copyright holder for this preprint (which was not certified by peer review) is the author/funder, who has granted bioRxiv a license to display the preprint in perpetuity. It is made available under aCC-BY-NC 4.0 International license.

Kazmierski *et al.*, Supplementary Figure 2

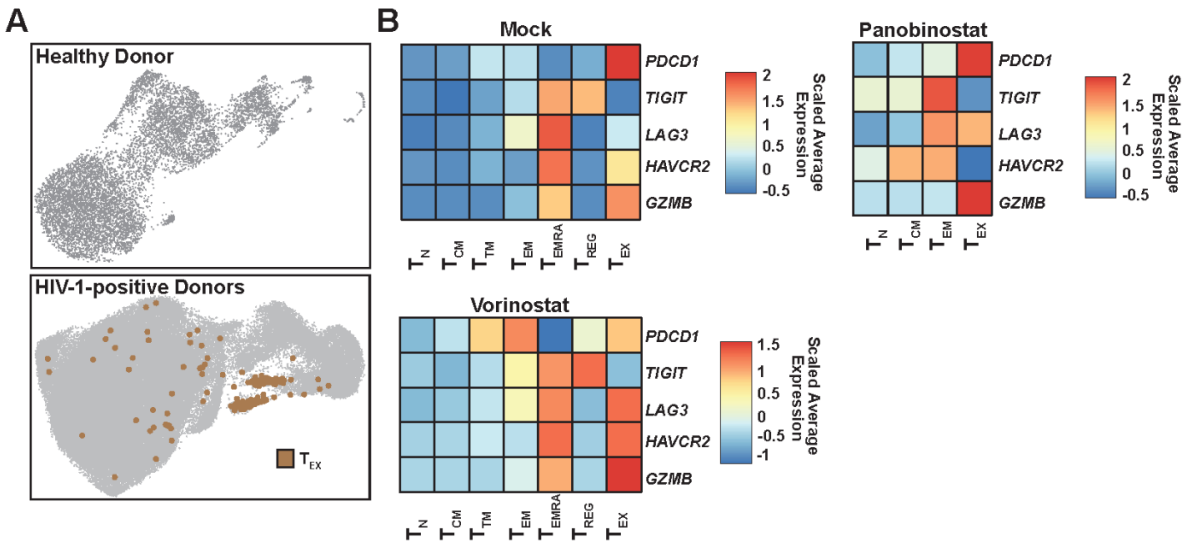

Supplementary Figure 2. A subset of CD4⁺ T-cells, identified specifically in cells isolated from PLHIV, resembles T_{EMRA} cells, with additional expression of the exhaustion marker *PDCD1*

(**A**) UMAP plots of CD4⁺ T-cells from an HIV-1-negative donor (n=1) and from aviremic PLHIV (n=3). Exhausted T-cells are coloured in brown.

(**B**) Heatmaps showing the scaled average expression of T-cell exhaustion markers, *PDCD1*, *TIGIT1*, *LAG3*, *HAVCR2*, *GZMB* in the different CD4⁺ T-cell subsets of PLHIV (n=3) upon mock-treatment or treatment with Vorinostat or Panobinostat.

bioRxiv preprint doi: https://doi.org/10.1101/2020.05.04.075119; this version posted June 4, 2023. The copyright holder for this preprint (which was not certified by peer review) is the author/funder, who has granted bioRxiv a license to display the preprint in perpetuity. It is made available under aCC-BY-NC 4.0 International license.

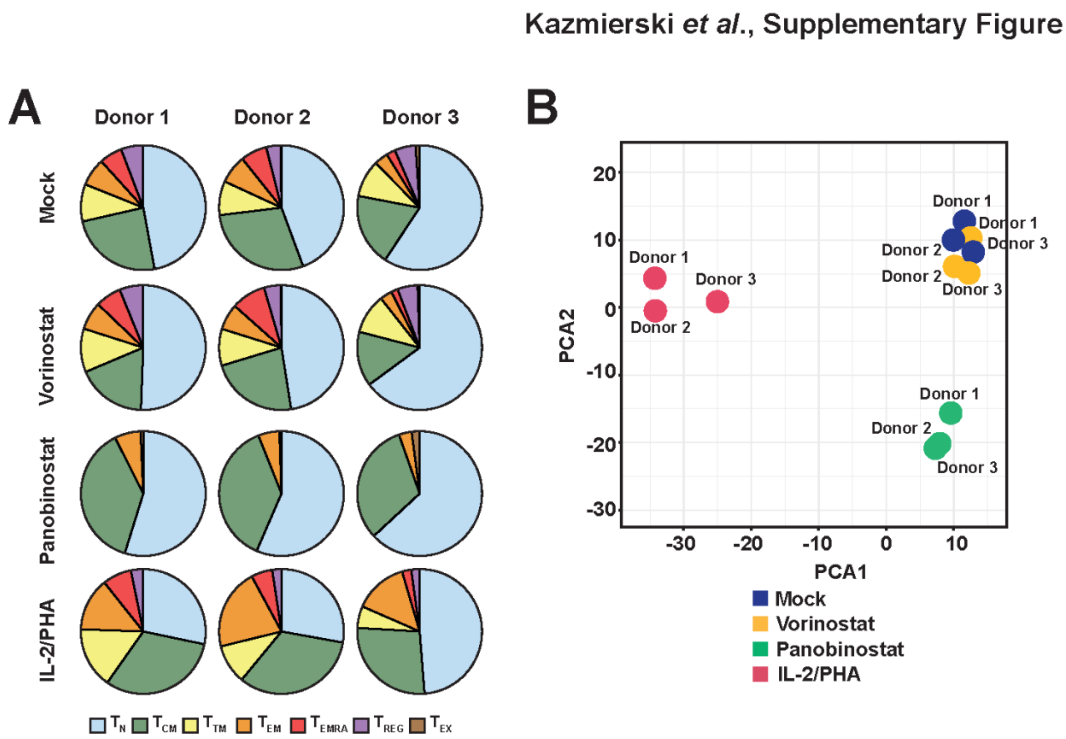

Supplementary Figure 3. CD4⁺ T-cell subset distribution and the transcriptomic landscape is determined by treatment condition in a donor-independent manner

(**A**) Pie charts displaying the CD4⁺ T-cell subset distribution of samples obtained from the individual PLHIV after indicated treatment.

(**B**) PCA based on the global gene expression profile of the individual samples after indicated treatment.

bioRxiv preprint doi: https://doi.org/10.1101/2020.05.04.075119; this version posted June 4, 2023. The copyright holder for this preprint (which was not certified by peer review) is the author/funder, who has granted bioRxiv a license to display the preprint in perpetuity. It is made available under aCC-BY-NC 4.0 International license.

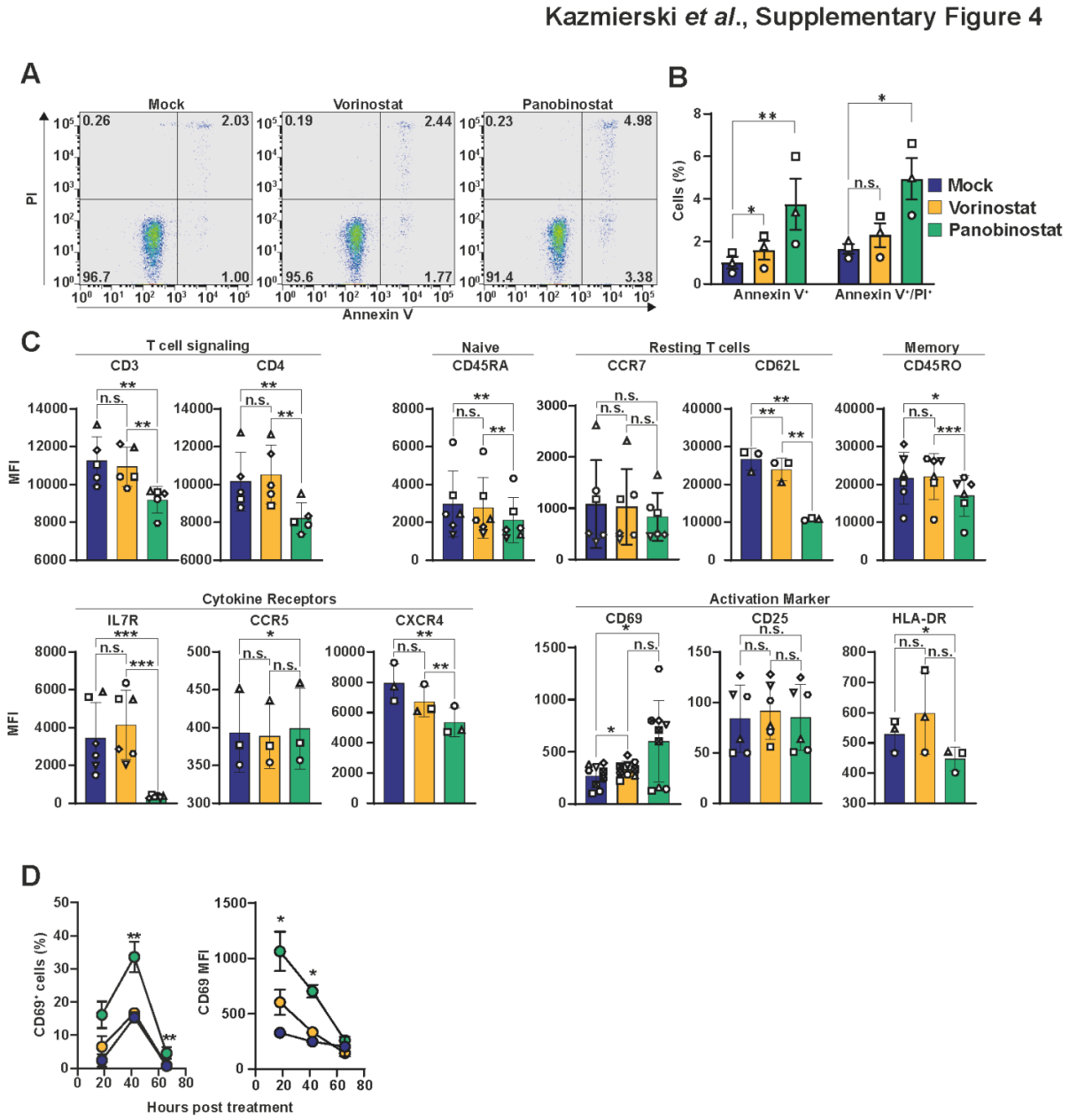

Supplementary Figure 4. Panobinostat treatment modulates expression of CD4⁺ T-cell markers

CD4⁺ T-cells from HIV-1-negative donors were treated *ex vivo* with 0.5% DMSO (mock), Vorinostat (500 nM) or Panobinostat (50 nM).

(**A**) Representative Annexin V/PI cell apoptosis staining upon indicated treatment for 48 hours.

(**B**) Percentage of Annexin V⁺- and Annexin V⁺/PI⁺-positive CD4⁺ T-cells from three individual donors upon indicated treatment for 48 hours.

bioRxiv preprint doi: https://doi.org/10.1101/2020.05.04.075119; this version posted June 4, 2023. The copyright holder for this preprint (which was not certified by peer review) is the author/funder, who has granted bioRxiv a license to display the preprint in perpetuity. It is made available under aCC-BY-NC 4.0 International license.

(**C**) Mean fluorescence intensity (MFI) of cell surface expression of indicated proteins upon indicated treatment for 48 hours.

(**D**) Percentage of $CD69^{+}$ T-cells and MFI of CD69 expression upon indicated treatment of cells from three donors.

bioRxiv preprint doi: https://doi.org/10.1101/2020.05.04.075119; this version posted June 4, 2023. The copyright holder for this preprint (which was not certified by peer review) is the author/funder, who has granted bioRxiv a license to display the preprint in perpetuity. It is made available under aCC-BY-NC 4.0 International license.

Kazmierski *et al.*, Supplementary Figure 5

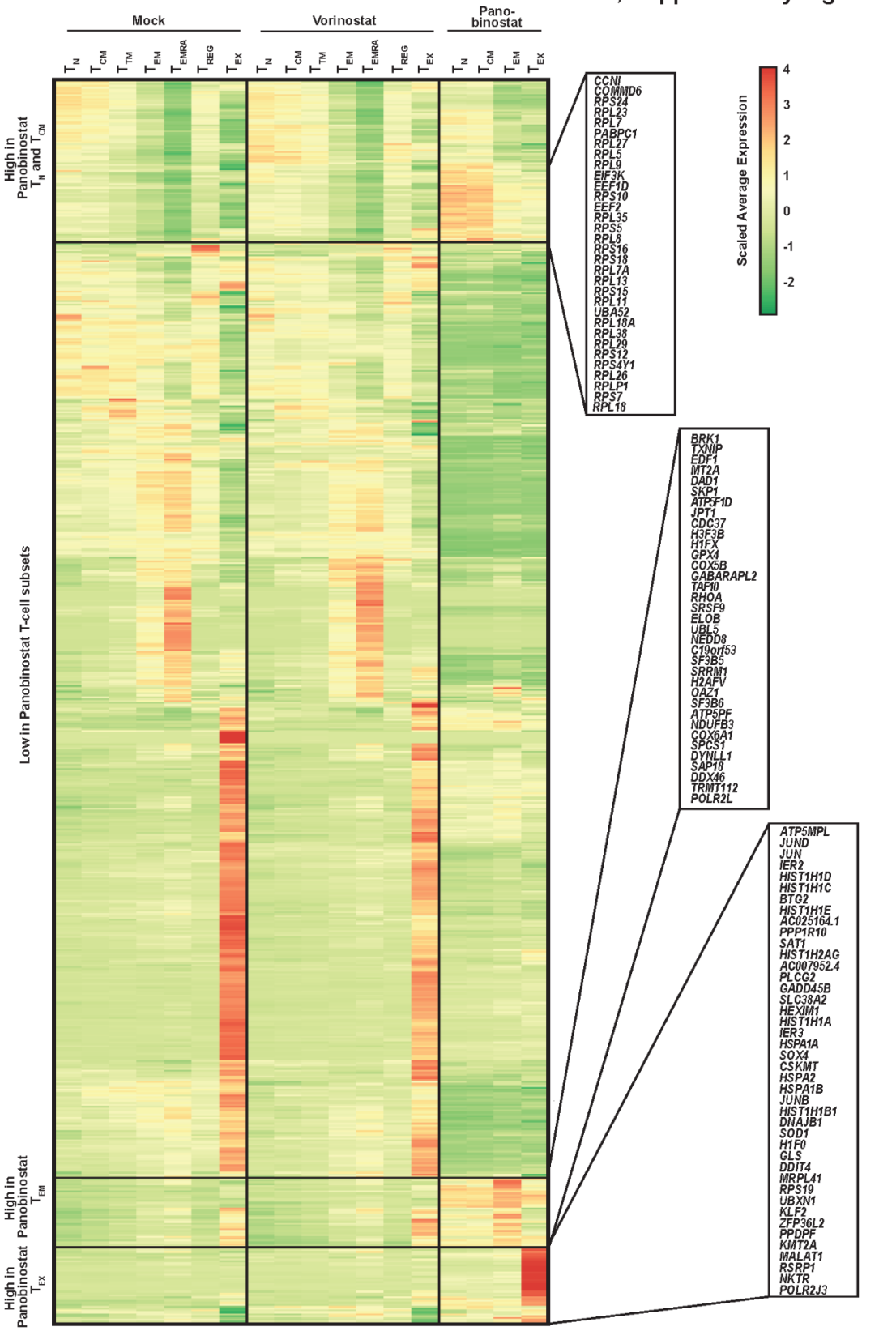

bioRxiv preprint doi: https://doi.org/10.1101/2020.05.04.075119; this version posted June 4, 2023. The copyright holder for this preprint (which was not certified by peer review) is the author/funder, who has granted bioRxiv a license to display the preprint in perpetuity. It is made available under aCC-BY-NC 4.0 International license.

Supplementary Figure 5. DEG analysis in CD4⁺ T-cell subsets

Heatmap showing all genes with statistically significant ($p< 0.05$) differential gene expression between one treatment as opposed to all other treatments (cut-off fold change 2). Groups of genes highly expressed in different T-cell subsets after Panobinostat treatment are highlighted.

bioRxiv preprint doi: https://doi.org/10.1101/2020.05.04.075119; this version posted June 4, 2023. The copyright holder for this preprint (which was not certified by peer review) is the author/funder, who has granted bioRxiv a license to display the preprint in perpetuity. It is made available under aCC-BY-NC 4.0 International license.

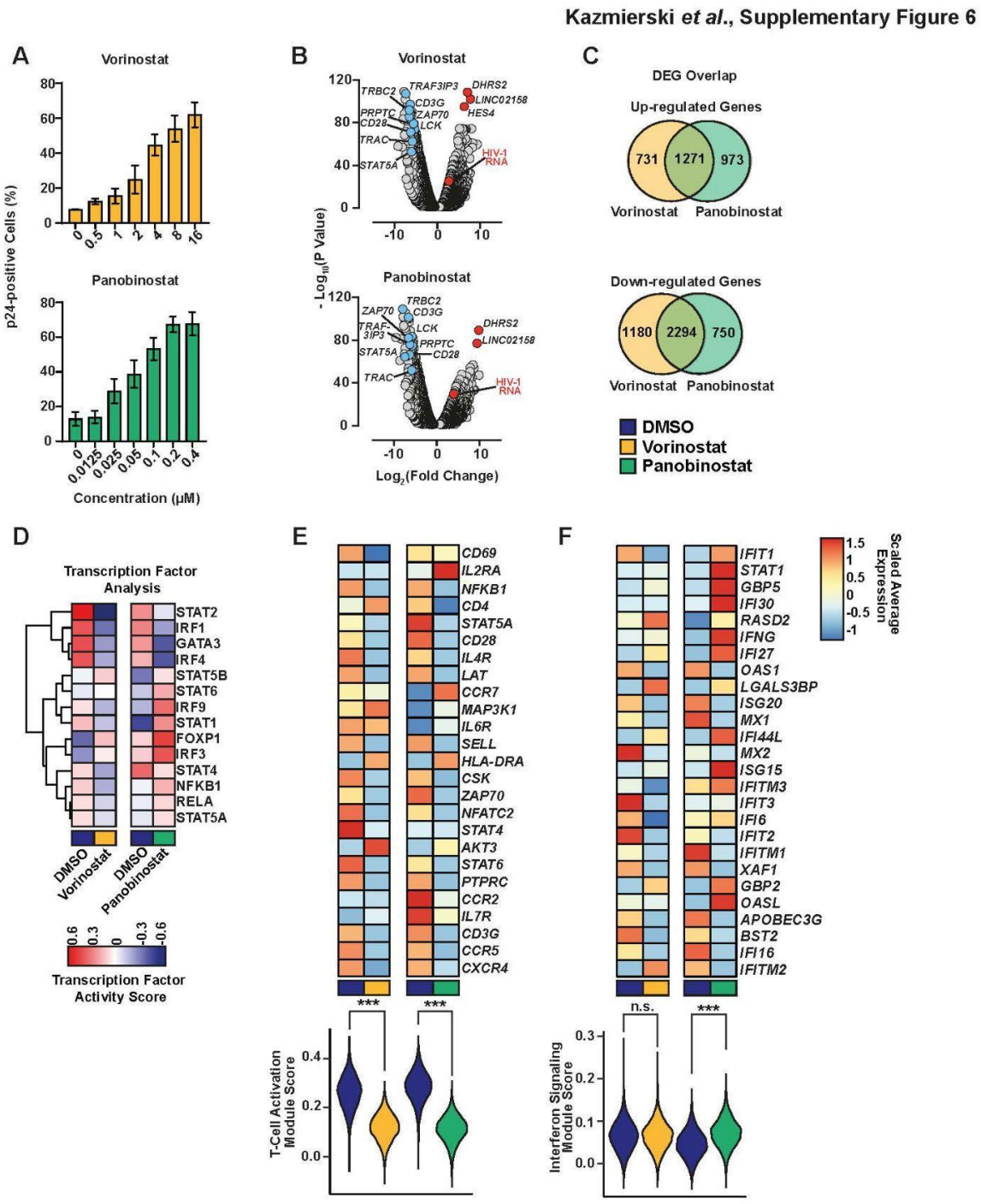

Supplementary Figure 6. HDACi-induced transcriptome in the J1.1 T-cell model of HIV-1 latency

(**A**) J1.1 T-cells were treated with the indicated concentration of Vorinostat or Panobinostat for 40 hours before quantification of intracellular HIV-1 p24 CA expression by flow cytometry.

bioRxiv preprint doi: https://doi.org/10.1101/2020.05.04.075119; this version posted June 4, 2023. The copyright holder for this preprint (which was not certified by peer review) is the author/funder, who has granted bioRxiv a license to display the preprint in perpetuity. It is made available under aCC-BY-NC 4.0 International license.

(**B**) - (**F**) J1.1 T-cells were treated with 16 µM Vorinostat, 1.6% DMSO (DMSO I), 200 nM Panobinostat or 0.2% DMSO (DMSO II) for 40 hours prior to single cell RNA-sequencing analysis.

(**B**) Volcano plot showing significant DEGs of Vorinostat- or Panobinostat-treated samples compared to mock samples.

(**C**) Overlap of genes up- and down-regulated after Vorinostat- or Panobinostat-treatment compared to mock-treatment.

(**D**) Activity analysis of selected transcription factors.

(**E**) Heatmap showing expression of selected genes involved in T-cell activation and signaling and T-cell activation module scores. Statistical significance for the module score was tested using Wilcoxon signed-rank testing.

(**F**) Heatmap showing expression of selected ISGs and IFN signaling module scores. Statistical significance for the module score was tested using Wilcoxon signed-rank testing.

bioRxiv preprint doi: https://doi.org/10.1101/2020.05.04.075119; this version posted June 4, 2023. The copyright holder for this preprint (which was not certified by peer review) is the author/funder, who has granted bioRxiv a license to display the preprint in perpetuity. It is made available under aCC-BY-NC 4.0 International license.

Kazmierski *et al.*, Supplementary Figure 7

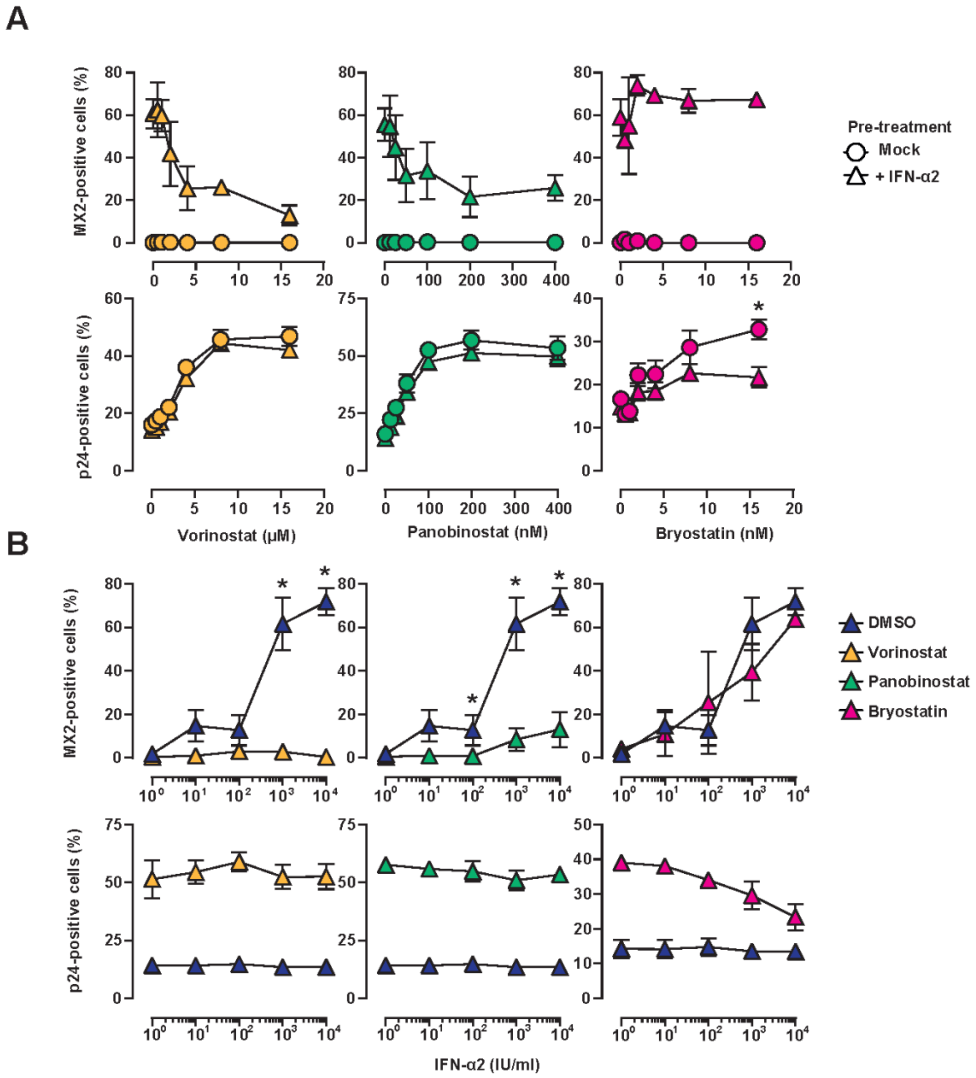

Supplementary Figure 7. HDAC inhibition suppresses type I interferon-induced ISG expression

(**A**) J1.1 T-cells were pre-treated with IFN-α2a (500 IU/ml) or mock-treated for 24 hours before incubation with indicated concentrations of Panobinostat, Vorinostat, Bryostatin or DMSO. Intracellular HIV-1 p24 CA and MX2 expression was quantified 40 hours post addition of LRAs by flow cytometry.

(**B**) J1.1 T-cells were cultured in the presence of Panobinostat (200 nM), Vorinostat (8 μM), Bryostatin (10 nM) or DMSO in combination with indicated concentrations of IFN-α2a. Intracellular HIV-1 p24 CA and MX2 expression was quantified after 40 hours.

bioRxiv preprint doi: https://doi.org/10.1101/2020.05.04.075119; this version posted June 4, 2023. The copyright holder for this preprint (which was not certified by peer review) is the author/funder, who has granted bioRxiv a license to display the preprint in perpetuity. It is made available under aCC-BY-NC 4.0 International license.

Experiments were performed as 3-4 independent replicates.

bioRxiv preprint doi: https://doi.org/10.1101/2020.05.04.075119; this version posted June 4, 2023. The copyright holder for this preprint (which was not certified by peer review) is the author/funder, who has granted bioRxiv a license to display the preprint in perpetuity. It is made available under aCC-BY-NC 4.0 International license.

Supplementary Table 1. Clinical data of the three PLHIV.

Shown are the dates of infection and ART initiation as well as viral loads and counts of $CD4^+$ T-cells in the peripheral blood. The detection limit for viral copies/ml is 50; samples with undetectable levels are indicated with "< 50".

Supplementary Table 2. DEGs in HIV-1-RNA-high and HIV-1-RNA-low J1.1 T-cells

Lists of genes that were differentially expressed in HIV-1-RNA-high and HIV-1-RNA-low J1.1 T-cells within each treatment (referring to Fig. 4E).

Supplementary Table 3. HIV-1 isolate sequences used for donor-specific mapping

List of HIV-1 proviral sequences that were used for donor-specific identification of HIV-1 reads (referring to Fig. 5A-B).

Supplementary Table 4. DEGs in HIV-1-RNA-positive and HIV-1-RNA-negative $CD4^+$ T-cells

Lists of genes that were differentially expressed in HIV-1-RNA-positive and HIV-1-RNA-negative $CD4^+$ T-cells (referring to Fig. 5F).

bioRxiv preprint doi: https://doi.org/10.1101/2020.05.04.075119; this version posted June 4, 2023. The copyright holder for this preprint (which was not certified by peer review) is the author/funder, who has granted bioRxiv a license to display the preprint in perpetuity. It is made available under aCC-BY-NC 4.0 International license.

References

1. Vanhamel, J., Bruggemans, A. & Debyser, Z. Establishment of latent HIV-1 reservoirs: what do we really know? *J Virus Erad* **5**, 3–9 (2019).
2. Hurst, J. *et al.* Immunological biomarkers predict HIV-1 viral rebound after treatment interruption. *Nat. Commun.* **6**, 8495 (12/2015).
3. Buzon, M. J. *et al.* HIV-1 persistence in CD4+ T cells with stem cell-like properties. *Nat. Med.* **20**, 139–142 (2014).
4. Chomont, N. *et al.* HIV reservoir size and persistence are driven by T cell survival and homeostatic proliferation. *Nat. Med.* **15**, 893–900 (8/2009).
5. Chavez, L., Calvanese, V. & Verdin, E. HIV Latency Is Established Directly and Early in Both Resting and Activated Primary CD4 T Cells. *PLoS Pathog.* **11**, e1004955 (2015).
6. Gantner, P. *et al.* HIV rapidly targets a diverse pool of CD4+ T cells to establish productive and latent infections. *Immunity* (2023) doi:10.1016/j.immuni.2023.01.030.
7. Abdel-Mohsen, M. *et al.* Recommendations for measuring HIV reservoir size in cure-directed clinical trials. *Nat. Med.* **26**, 1339–1350 (2020).
8. Finzi, D. *et al.* Latent infection of CD4+ T cells provides a mechanism for lifelong persistence of HIV-1, even in patients on effective combination therapy. *Nat. Med.* **5**, 512–517 (1999).
9. Siliciano, J. D. *et al.* Long-term follow-up studies confirm the stability of the latent reservoir for HIV-1 in resting CD4+ T cells. *Nat. Med.* **9**, 727–728 (2003).
10. Cohn, L. B. *et al.* HIV-1 Integration Landscape during Latent and Active Infection. *Cell* **160**, 420–432 (01/2015).
11. von Stockenstrom, S. *et al.* Longitudinal Genetic Characterization Reveals That Cell Proliferation Maintains a Persistent HIV Type 1 DNA Pool During Effective HIV Therapy. *J. Infect. Dis.* **212**, 596–607 (2015).
12. Wagner, T. A. *et al.* Proliferation of cells with HIV integrated into cancer genes contributes to persistent infection. *Science* **345**, 570–573 (08/2014).

bioRxiv preprint doi: https://doi.org/10.1101/2020.05.04.075119; this version posted June 4, 2023. The copyright holder for this preprint (which was not certified by peer review) is the author/funder, who has granted bioRxiv a license to display the preprint in perpetuity. It is made available under aCC-BY-NC 4.0 International license.

13. Cohn, L. B. *et al.* Clonal CD4+ T cells in the HIV-1 latent reservoir display a distinct gene profile upon reactivation. *Nat. Med.* **24**, 604–609 (5/2018).
14. Kim, Y., Anderson, J. L. & Lewin, S. R. Getting the 'Kill' into 'Shock and Kill': Strategies to Eliminate Latent HIV. *Cell Host Microbe* **23**, 14–26 (01/2018).
15. Margolis, D. M., Garcia, J. V., Hazuda, D. J. & Haynes, B. F. Latency reversal and viral clearance to cure HIV-1. *Science* **353**, aaf6517 (2016).
16. Archin, N. M. *et al.* Administration of vorinostat disrupts HIV-1 latency in patients on antiretroviral therapy. *Nature* **487**, 482–485 (2012).
17. Elliott, J. H. *et al.* Activation of HIV transcription with short-course vorinostat in HIV-infected patients on suppressive antiretroviral therapy. *PLoS Pathog.* **10**, e1004473 (2014).
18. Søgaard, O. S. *et al.* The Depsipeptide Romidepsin Reverses HIV-1 Latency In Vivo. *PLoS Pathog.* **11**, e1005142 (2015).
19. Rasmussen, T. A. *et al.* Panobinostat, a histone deacetylase inhibitor, for latent-virus reactivation in HIV-infected patients on suppressive antiretroviral therapy: a phase 1/2, single group, clinical trial. *The Lancet HIV* **1**, e13–e21 (10/2014).
20. Nixon, C. C. *et al.* Systemic HIV and SIV latency reversal via non-canonical NF-κB signalling in vivo. *Nature* **578**, 160–165 (2020).
21. McBrien, J. B. *et al.* Robust and persistent reactivation of SIV and HIV by N-803 and depletion of CD8+ cells. *Nature* **578**, 154–159 (2020).
22. Grau-Expósito, J. *et al.* Latency reversal agents affect differently the latent reservoir present in distinct CD4+ T subpopulations. *PLoS Pathog.* **15**, e1007991 (2019).
23. Archin, N. M. *et al.* Expression of latent HIV induced by the potent HDAC inhibitor suberoylanilide hydroxamic acid. *AIDS Res. Hum. Retroviruses* **25**, 207–212 (2009).
24. Rasmussen, T. A. *et al.* Comparison of HDAC inhibitors in clinical development: Effect on HIV production in latently infected cells and T-cell activation. *Hum. Vaccin. Immunother.* **9**, 993–1001 (2013).
25. Mahnke, Y. D., Brodie, T. M., Sallusto, F., Roederer, M. & Lugli, E. The who's who of T-

bioRxiv preprint doi: https://doi.org/10.1101/2020.05.04.075119; this version posted June 4, 2023. The copyright holder for this preprint (which was not certified by peer review) is the author/funder, who has granted bioRxiv a license to display the preprint in perpetuity. It is made available under aCC-BY-NC 4.0 International license.

cell differentiation: Human memory T-cell subsets: HIGHLIGHTS. *Eur. J. Immunol.* **43**, 2797–2809 (11/2013).

26. Cano-Gamez, E. *et al.* Single-cell transcriptomics identifies an effectorness gradient shaping the response of CD4+ T cells to cytokines. *Nat. Commun.* **11**, 1801 (12/2020).
27. Szabo, P. A. *et al.* Single-cell transcriptomics of human T cells reveals tissue and activation signatures in health and disease. *Nat. Commun.* **10**, 4706 (12/2019).
28. Breton, G. *et al.* Programmed death-1 is a marker for abnormal distribution of naive/memory T cell subsets in HIV-1 infection. *J. Immunol.* **191**, 2194–2204 (2013).
29. Wang, S. *et al.* An atlas of immune cell exhaustion in HIV-infected individuals revealed by single-cell transcriptomics. *Emerg. Microbes Infect.* **9**, 2333–2347 (2020).
30. Akimova, T., Beier, U. H., Liu, Y., Wang, L. & Hancock, W. W. Histone/protein deacetylases and T-cell immune responses. *Blood* **119**, 2443–2451 (2012).
31. Brinkmann, C. R. *et al.* Treatment of HIV-Infected Individuals with the Histone Deacetylase Inhibitor Panobinostat Results in Increased Numbers of Regulatory T Cells and Limits *Ex Vivo* Lipopolysaccharide-Induced Inflammatory Responses. *mSphere* **3**, (2018).
32. Perez, V. L. *et al.* An HIV-1-infected T cell clone defective in IL-2 production and Ca2+ mobilization after CD3 stimulation. *J. Immunol.* **147**, 3145–3148 (1991).
33. Symons, J. *et al.* HIV integration sites in latently infected cell lines: evidence of ongoing replication. *Retrovirology* **14**, 2 (12/2017).
34. Jamaluddin, M. S., Hu, P.-W., Jan, Y., Siwak, E. B. & Rice, A. P. Short Communication: The Broad-Spectrum Histone Deacetylase Inhibitors Vorinostat and Panobinostat Activate Latent HIV in CD4(+) T Cells In Part Through Phosphorylation of the T-Loop of the CDK9 Subunit of P-TEFb. *AIDS Res. Hum. Retroviruses* **32**, 169–173 (2016).
35. Grandvaux, N. *et al.* Transcriptional profiling of interferon regulatory factor 3 target genes: direct involvement in the regulation of interferon-stimulated genes. *J. Virol.* **76**, 5532–5539 (2002).
36. Perez, M. *et al.* Bryostatin-1 Synergizes with Histone Deacetylase Inhibitors to

bioRxiv preprint doi: https://doi.org/10.1101/2020.05.04.075119; this version posted June 4, 2023. The copyright holder for this preprint (which was not certified by peer review) is the author/funder, who has granted bioRxiv a license to display the preprint in perpetuity. It is made available under aCC-BY-NC 4.0 International license.

Reactivate HIV-1 from Latency. *CHR* **8**, 418–429 (2010).

37. Beans, E. J. *et al.* Highly potent, synthetically accessible prostratin analogs induce latent HIV expression in vitro and ex vivo. *Proceedings of the National Academy of Sciences* **110**, 11698–11703 (2013).
38. Wain-Hobson, S., Sonigo, P., Danos, O., Cole, S. & Alizon, M. Nucleotide sequence of the AIDS virus, LAV. *Cell* **40**, 9–17 (1985).
39. Liu, R. *et al.* Single-cell transcriptional landscapes reveal HIV-1–driven aberrant host gene transcription as a potential therapeutic target. *Sci. Transl. Med.* **12**, eaaz0802 (2020).
40. Srinivasachar Badarinarayan, S. *et al.* HIV-1 infection activates endogenous retroviral promoters regulating antiviral gene expression. *Nucleic Acids Res.* **48**, 10890–10908 (2020).
41. Qu, D. *et al.* Long noncoding RNA MALAT1 releases epigenetic silencing of HIV-1 replication by displacing the polycomb repressive complex 2 from binding to the LTR promoter. *Nucleic Acids Res.* **47**, 3013–3027 (2019).
42. Liu, H., Hu, P.-W., Couturier, J., Lewis, D. E. & Rice, A. P. HIV-1 replication in CD4+ T cells exploits the down-regulation of antiviral NEAT1 long non-coding RNAs following T cell activation. *Virology* **522**, 193–198 (2018).
43. Valente, S. T. & Goff, S. P. Inhibition of HIV-1 gene expression by a fragment of hnRNP U. *Mol. Cell* **23**, 597–605 (2006).
44. Garrus, J. E. *et al.* Tsg101 and the vacuolar protein sorting pathway are essential for HIV-1 budding. *Cell* **107**, 55–65 (2001).
45. Chatel-Chaix, L., Abrahamyan, L., Fréchina, C., Mouland, A. J. & DesGroseillers, L. The host protein Staufen1 participates in human immunodeficiency virus type 1 assembly in live cells by influencing pr55Gag multimerization. *J. Virol.* **81**, 6216–6230 (2007).
46. Milev, M. P., Brown, C. M. & Mouland, A. J. Live cell visualization of the interactions between HIV-1 Gag and the cellular RNA-binding protein Staufen1. *Retrovirology* **7**, 41 (2010).

bioRxiv preprint doi: https://doi.org/10.1101/2020.05.04.075119; this version posted June 4, 2023. The copyright holder for this preprint (which was not certified by peer review) is the author/funder, who has granted bioRxiv a license to display the preprint in perpetuity. It is made available under aCC-BY-NC 4.0 International license.

47. König, R. *et al.* Global analysis of host-pathogen interactions that regulate early-stage HIV-1 replication. *Cell* **135**, 49–60 (2008).
48. Tsai, P. *et al.* In vivo analysis of the effect of panobinostat on cell-associated HIV RNA and DNA levels and latent HIV infection. *Retrovirology* **13**, 36 (12/2016).
49. Bartholomeeusen, K., Fujinaga, K., Xiang, Y. & Peterlin, B. M. Histone deacetylase inhibitors (HDACis) that release the positive transcription elongation factor b (P-TEFb) from its inhibitory complex also activate HIV transcription. *J. Biol. Chem.* **288**, 14400–14407 (2013).
50. Khoury, G. *et al.* HIV latency reversing agents act through Tat post translational modifications. *Retrovirology* **15**, 36 (2018).
51. Kwaa, A. K. R., Talana, C. A. G. & Blankson, J. N. Interferon Alpha Enhances NK Cell Function and the Suppressive Capacity of HIV-Specific CD8+ T Cells. *J. Virol.* **93**, (2019).
52. Tomescu, C., Tebas, P. & Montaner, L. J. IFN-α augments natural killer-mediated antibody-dependent cellular cytotoxicity of HIV-1-infected autologous CD4+ T cells regardless of major histocompatibility complex class 1 downregulation. *AIDS* **31**, 613–622 (2017).
53. Edens, R. E., Dagtas, S. & Gilbert, K. M. Histone deacetylase inhibitors induce antigen specific anergy in lymphocytes: a comparative study. *Int. Immunopharmacol.* **6**, 1673–1681 (2006).
54. Pace, M. *et al.* Histone Deacetylase Inhibitors Enhance CD4 T Cell Susceptibility to NK Cell Killing but Reduce NK Cell Function. *PLoS Pathog.* **12**, e1005782 (2016).
55. Triplett, T. A., Holay, N., Kottapalli, S., VanDenBerg, C. & Capasso, A. Elucidating the Role of HDACs in T Cell Biology and Comparing Distinct HDAC Inhibitors in Augmenting Responses to Cancer Immunotherapy. *J. Immunol.* **204**, 165.23 (2020).
56. Jones, R. B. *et al.* Histone deacetylase inhibitors impair the elimination of HIV-infected cells by cytotoxic T-lymphocytes. *PLoS Pathog.* **10**, e1004287–e1004287 (2014).
57. Boucau, J., Das, J., Joshi, N. & Le Gall, S. Latency reversal agents modulate HIV

bioRxiv preprint doi: https://doi.org/10.1101/2020.05.04.075119; this version posted June 4, 2023. The copyright holder for this preprint (which was not certified by peer review) is the author/funder, who has granted bioRxiv a license to display the preprint in perpetuity. It is made available under aCC-BY-NC 4.0 International license.

antigen processing and presentation to CD8 T cells. *PLoS Pathog.* **16**, e1008442 (2020).

58. Blazkova, J. *et al.* Effect of Histone Deacetylase Inhibitors on HIV Production in Latently Infected, Resting CD4+ T Cells From Infected Individuals Receiving Effective Antiretroviral Therapy. *J. Infect. Dis.* **206**, 765–769 (2012).
59. Zerbato, J. M. *et al.* Multiply spliced HIV RNA is a predictive measure of virus production ex vivo and in vivo following reversal of HIV latency. *EBioMedicine* **65**, 103241 (2021).
60. Spivak, A. M. *et al. Ex Vivo* Bioactivity and HIV-1 Latency Reversal by Ingenol Dibenzoate and Panobinostat in Resting CD4 $^{+}$ T Cells from Aviremic Patients. *Antimicrob. Agents Chemother.* **59**, 5984–5991 (10/2015).
61. Lucera, M. B. *et al.* The Histone Deacetylase Inhibitor Vorinostat (SAHA) Increases the Susceptibility of Uninfected CD4+ T Cells to HIV by Increasing the Kinetics and Efficiency of Postentry Viral Events. *J. Virol.* **88**, 10803–10812 (2014).
62. Valenzuela-Fernández, A. *et al.* Histone deacetylase 6 regulates human immunodeficiency virus type 1 infection. *Mol. Biol. Cell* **16**, 5445–5454 (2005).
63. Smith, J. A., Yeung, J., Kao, G. D. & Daniel, R. A role for the histone deacetylase HDAC4 in the life-cycle of HIV-1-based vectors. *Virol. J.* **7**, 237 (2010).
64. Ran, X., Ao, Z., Olukitibi, T. & Yao, X. Characterization of the Role of Host Cellular Factor Histone Deacetylase 10 during HIV-1 Replication. *Viruses* **12**, (2019).
65. Marrero-Hernández, S. *et al.* HIV-1 Nef Targets HDAC6 to Assure Viral Production and Virus Infection. *Front. Microbiol.* **10**, 2437 (2019).
66. Bode, K. A. *et al.* Histone deacetylase inhibitors decrease Toll-like receptor-mediated activation of proinflammatory gene expression by impairing transcription factor recruitment. *Immunology* **122**, 596–606 (12/2007).
67. Shakespear, M. R., Halili, M. A., Irvine, K. M., Fairlie, D. P. & Sweet, M. J. Histone deacetylases as regulators of inflammation and immunity. *Trends Immunol.* **32**, 335–343 (7/2011).
68. White, C. H. *et al.* Transcriptional Modulation of Human Endogenous Retroviruses in

bioRxiv preprint doi: https://doi.org/10.1101/2020.05.04.075119; this version posted June 4, 2023. The copyright holder for this preprint (which was not certified by peer review) is the author/funder, who has granted bioRxiv a license to display the preprint in perpetuity. It is made available under aCC-BY-NC 4.0 International license.

Primary CD4+ T Cells Following Vorinostat Treatment. *Front. Immunol.* **9**, 603 (2018).

69. Krönung, S. K. *et al.* LTR12 promoter activation in a broad range of human tumor cells by HDAC inhibition. *Oncotarget* **7**, 33484–33497 (2016).
70. Bruner, K. M. *et al.* Defective proviruses rapidly accumulate during acute HIV-1 infection. *Nat. Med.* **22**, 1043–1049 (2016).
71. Bruner, K. M. *et al.* A quantitative approach for measuring the reservoir of latent HIV-1 proviruses. *Nature* vol. 566 120–125 Preprint at https://doi.org/10.1038/s41586-019-0898-8 (2019).
72. Ho, Y.-C. *et al.* Replication-competent noninduced proviruses in the latent reservoir increase barrier to HIV-1 cure. *Cell* **155**, 540–551 (2013).
73. Einkauf, K. B. *et al.* Parallel analysis of transcription, integration, and sequence of single HIV-1 proviruses. *Cell* **185**, 266–282.e15 (2022).
74. Wu, V. H. *et al.* Profound phenotypic and epigenetic heterogeneity of the HIV-1-infected CD4+ T cell reservoir. *Nat. Immunol.* **24**, 359–370 (2023).
75. Clark, I. C. *et al.* HIV silencing and cell survival signatures in infected T cell reservoirs. *Nature* **614**, 318–325 (2023).
76. Collora, J. A. *et al.* Single-cell multiomics reveals persistence of HIV-1 in expanded cytotoxic T cell clones. *Immunity* **55**, 1013–1031.e7 (2022).
77. Hsieh, P.-C. *et al.* p53 downstream target DDA3 is a novel microtubule-associated protein that interacts with end-binding protein EB3 and activates beta-catenin pathway. *Oncogene* **26**, 4928–4940 (2007).
78. Kwon, H. J., Park, J. E., Song, H. & Jang, C.-Y. DDA3 and Mdp3 modulate Kif2a recruitment onto the mitotic spindle to control minus-end spindle dynamics. *J. Cell Sci.* **129**, 2719–2725 (2016).
79. Swearingen, M. L., Sun, D., Bourner, M. & Weinstein, E. J. Detection of differentially expressed HES-6 gene in metastatic colon carcinoma by combination of suppression subtractive hybridization and cDNA library array. *Cancer Lett.* **198**, 229–239 (2003).
80. Vias, M. *et al.* Pro-neural transcription factors as cancer markers. *BMC Med. Genomics*

bioRxiv preprint doi: https://doi.org/10.1101/2020.05.04.075119; this version posted June 4, 2023. The copyright holder for this preprint (which was not certified by peer review) is the author/funder, who has granted bioRxiv a license to display the preprint in perpetuity. It is made available under aCC-BY-NC 4.0 International license.

1, 17 (2008).

81. Bill, C. A. & Vines, C. M. Phospholipase C. *Adv. Exp. Med. Biol.* **1131**, 215–242 (2020).
82. Spadaro, F. *et al.* Nuclear phosphoinositide-specific phospholipase C β1 controls cytoplasmic CCL2 mRNA levels in HIV-1 gp120-stimulated primary human macrophages. *PLoS One* **8**, e59705 (2013).
83. Machnowska, P. *et al.* Prevalence and persistence of transmitted drug resistance mutations in the German HIV-1 Seroconverter Study Cohort. *PLoS One* **14**, e0209605 (2019).
84. Butler, A., Hoffman, P., Smibert, P., Papalexi, E. & Satija, R. Integrating single-cell transcriptomic data across different conditions, technologies, and species. *Nat. Biotechnol.* **36**, 411–420 (2018).
85. MacLeod, M. K. L., Clambey, E. T., Kappler, J. W. & Marrack, P. CD4 memory T cells: what are they and what can they do? *Semin. Immunol.* **21**, 53–61 (2009).
86. Pušnik, J. *et al.* Expansion of Stem Cell-Like CD4+ Memory T Cells during Acute HIV-1 Infection Is Linked to Rapid Disease Progression. *J. Virol.* **93**, (2019).
87. Kononchik, J. *et al.* HIV-1 targets L-selectin for adhesion and induces its shedding for viral release. *Nat. Commun.* **9**, 2825 (2018).
88. Golubovskaya, V. & Wu, L. Different Subsets of T Cells, Memory, Effector Functions, and CAR-T Immunotherapy. *Cancers* **8**, (2016).
89. Tian, Y. *et al.* Unique phenotypes and clonal expansions of human CD4 effector memory T cells re-expressing CD45RA. *Nat. Commun.* **8**, 1473 (2017).
90. Jain, N., Nguyen, H., Chambers, C. & Kang, J. Dual function of CTLA-4 in regulatory T cells and conventional T cells to prevent multiorgan autoimmunity. *Proc. Natl. Acad. Sci. U. S. A.* **107**, 1524–1528 (2010).
91. Jiang, Y., Li, Y. & Zhu, B. T-cell exhaustion in the tumor microenvironment. *Cell Death Dis.* **6**, e1792 (2015).
92. Ramírez, F. *et al.* deepTools2: a next generation web server for deep-sequencing data analysis. *Nucleic Acids Res.* **44**, W160–5 (2016).

bioRxiv preprint doi: https://doi.org/10.1101/2020.05.04.075119; this version posted June 4, 2023. The copyright holder for this preprint (which was not certified by peer review) is the author/funder, who has granted bioRxiv a license to display the preprint in perpetuity. It is made available under aCC-BY-NC 4.0 International license.

93. Metsalu, T. & Vilo, J. ClustVis: a web tool for visualizing clustering of multivariate data using Principal Component Analysis and heatmap. *Nucleic Acids Res.* **43**, W566–70 (2015).
94. Wang, J., Duncan, D., Shi, Z. & Zhang, B. WEB-based GEne SeT AnaLysis Toolkit (WebGestalt): update 2013. *Nucleic Acids Res.* **41**, W77–83 (2013).
95. Zhang, B., Kirov, S. & Snoddy, J. WebGestalt: an integrated system for exploring gene sets in various biological contexts. *Nucleic Acids Res.* **33**, W741–8 (2005).
96. Mi, H. & Thomas, P. PANTHER pathway: an ontology-based pathway database coupled with data analysis tools. *Methods Mol. Biol.* **563**, 123–140 (2009).
97. Garcia-Alonso, L., Holland, C. H., Ibrahim, M. M., Turei, D. & Saez-Rodriguez, J. Benchmark and integration of resources for the estimation of human transcription factor activities. *Genome Res.* **29**, 1363–1375 (2019).
98. Holland, C. H. *et al.* Robustness and applicability of transcription factor and pathway analysis tools on single-cell RNA-seq data. *Genome Biol.* **21**, 36 (2020).
99. Jassal, B. *et al.* The reactome pathway knowledgebase. *Nucleic Acids Res.* **48**, D498–D503 (2020).
100. Liberzon, A. *et al.* Molecular signatures database (MSigDB) 3.0. *Bioinformatics* **27**, 1739–1740 (2011).
101. Lun, A., Risso, D., Korthauer, K. & Others. SingleCellExperiment: S4 classes for single cell data. *R package version* **1**, (2019).
102. Lun, A. T. L., McCarthy, D. J. & Marioni, J. C. A step-by-step workflow for low-level analysis of single-cell RNA-seq data with Bioconductor. *F1000Res.* **5**, 2122 (2016).